SIAM J. Applied Dynamical Systems
Vol. xx, pp. x



# Existence, Stability, and Dynamics of Ring and Near-Ring Solutions to the Saturated Gierer-Meinhardt Model in the Semi-Strong Regime

Iain R. Moyles[†] and Michael J. Ward[‡]

**Abstract.** We analyze a singularly perturbed reaction-diffusion system in the semi-strong diffusion regime in two spatial dimensions where an activator species is localized to a closed curve, while the inhibitor species exhibits long range behavior over the domain. In the limit of small activator diffusivity we derive a new moving boundary problem characterizing the slow time evolution of the curve, which is defined in terms of a quasi steady-state inhibitor diffusion field and its properties on the curve. Numerical results from this curve evolution problem are illustrated for the Gierer-Meinhardt model (GMS) with saturation in the activator kinetics. A detailed analysis of the existence, stability, and dynamics of ring and near-ring solutions for the GMS model is given, whereby the activator concentrates on a thin ring concentric within a circular domain. A key new result for this ring geometry is that by including activator saturation there is a qualitative change in the phase portrait of ring equilibria, in that there is an $S$-shaped bifurcation diagram for ring equilibria, which allows for hysteresis behavior. In contrast, without saturation, it is well-known that there is a saddle-node bifurcation for the ring equilibria. For a near-circular ring, we develop an asymptotic expansion up to quadratic order to fully characterize the normal velocity perturbations from our curve-evolution problem. In addition, we also analyze the linear stability of the ring solution to both breakup instabilities, leading to the disintegration of a ring into localized spots, and zig-zag instabilities, leading to the slow shape deformation of the ring. We show from a nonlocal eigenvalue problem that activator saturation can stabilize breakup patterns that otherwise would be unstable. Through a detailed matched asymptotic analysis, we derive a new explicit formula for the small eigenvalues associated with zig-zag instabilities, and we show that they are equivalent to the velocity perturbations induced by the near-circular ring geometry. Finally, we present full numerical simulations from the GMS PDE system that confirm the predictions of the analysis.

**Key words.** homoclinic orbits, zig-zag instability, nonlocal eigenvalue problem, WKB stability, hysteresis

**AMS subject classifications.** 35B25, 35B32, 35B36, 35B40, 35K57, 35P30, 35Q92, 37M20, 37N25

## 1. Introduction.

Modern biological pattern formation is generally posited mathematically via coupled reaction-diffusion (RD) systems where some spatially homogeneous solution exists for a set of reaction kinetics. Often the effect of spatial diffusion in such systems is to initiate spatially inhomogeneous patterns from perturbations of the otherwise stable steady-states of the reaction kinetics. Classically, the onset of such spatial solutions can be analyzed using a criterion derived by Turing (cf. [38]). However, large amplitude spatially inhomogeneous patterns can persist beyond what one would anticipate from a Turing-type analysis, and it is of general interest to study such patterns far from this Turing regime.

An early two-component RD model for complex pattern formation was developed in [12] and is known as the Gierer-Meinhardt (GM) model. This model couples an autocatalytic short

[†]MACSI, University of Limerick, Limerick, Ireland (iain.moyles@ul.ie). This author was supported by a Vanier Canada Graduate Scholarship. He is grateful to funding from a Science Foundation Ireland Grant SFI/13/IA/1923 during the preparation of this manuscript.

[‡]Institute of Applied Mathematics, University of British Columbia, Vancouver, BC, Canada, V6T 1Z2 (mward@math.ubc.ca). This author was supported by the NSERC Discovery Grant 81541.

range activator with a long range inhibitor, and leads to self-sustaining patterns that are used to model biological morphogenesis. This model has been used as a basis for explaining the formation of embryonic axes, of leaf formation at the tip of a growing shoot, and of shell patterns on mollusks (cf. [12], [16], [24], [34]). Aside from the GM models, there are various other models that exhibit complex and interesting pattern dynamics. These include the Gray-Scott (GS) model of theoretical chemistry (cf. [30], [31], [33], [7]), a hybrid chemotaxis RD model of fish skin patterns (cf. [32]), the Swift-Hohenberg model (cf. [13]), a generalized Schnakenberg system modelling root hair initiation in plants (cf. [5]), a model for urban crime (cf. [37]), and many more. Many of these models admit similar structures and patterns due to the coupling of short range activation and long range inhibition.

Many two-component pattern formation models exhibiting localized patterns can be written in terms of an activator $v$ and an inhibitor $u$ in the singularly perturbed dimensionless form

$$v_t = \epsilon^2 \Delta v - v + g(u,v)\,, \qquad \tau u_t = D\Delta u - u + \frac{1}{\epsilon} f(u,v)\,, \tag{1.1}$$

on some domain $\Omega \subset \mathbb{R}^2$ subject to Neumann boundary conditions on the boundary $\partial\Omega$. Some specific studies in more than two dimensions can be found in [22] and [29]. In (1.1), $\tau$ is an effective time scale delay between the activator and inhibitor, while $D$ and $\epsilon^2$, with $\epsilon \ll 1$, are the inhibitor and activator diffusivities respectively. We will consider a classical limit for this problem, the so-called semi-strong regime where $D = \mathcal{O}(1)$. With this formulation, the activator is singularly perturbed and localized, owing to its small diffusivity, while the inhibitor has a longer range behaviour. The functions $f(u,v)$ and $g(u,v)$, with $g(u,0) = 0$ and $f(u,0) = 0$, are chosen such that spatially homogeneous steady-states are unstable to a standard Turing analysis [38].

In the simpler setting of a one-dimensional spatial domain, there has been a plethora of work characterizing the existence, stability, and the dynamics of steady-state and quasi-steady state solutions to the GM, GS, and Schnakenberg, models (cf. [6], [8], [9], [15], [14], [18], [27], [30], [40], [41], [42]). For the two-dimensional GM model, straight stripe patterns in rectangular domains have been studied (cf. [17], [25], [10]). In higher dimensions, the existence of steady-state ring solutions in $N$-dimensional radially symmetric domains was investigated in [29], without any stability analysis. Ring solutions were analyzed in [25], [20], [21] and the linear stability analysis of such solutions to a breakup instability, which triggers the disintegration of a ring into localized spots, relied on studying the spectrum of a non-local eigenvalue problem (NLEP). In certain special cases, the analysis of the NLEP can be reduced to the much simpler problem of analyzing an explicit transcendental equation for the eigenvalue parameter (cf. [25], [28]).

The general form of the reaction kinetics for the GM model are

$$f(u,v) = \frac{v^o}{u^s}\,, \qquad g(u,v) = \frac{v^p}{u^q(1+\sigma v^p)}\,, \tag{1.2}$$

where $\sigma \geq 0$ is a saturation parameter, which limits the autocatalytic activation of $v$. For the range $\sigma > 0$ the model is generally referred to as the saturated Gierer-Meinhardt (GMS) model. Although most of the previous analytical studies of the GM model is for the basic model with $\sigma = 0$, there are a few studies that allow for saturation. For the case where the

activator is localized on the midline of a rectangular domain, resulting in a straight stripe pattern, [17] provides existence and stability results for a stripe for the GMS model. However, there are no corresponding studies where the activator concentrates on a circular curve, i.e. a ring pattern, or on arbitrary curves. In a one-dimensional domain, some existence and stability results for a spike solution to the GMS model are presented in [43] for the so-called shadow regime, where $D \to \infty$, with the authors conceding that the establishment of similar stability results for finite $D$ is an open problem.

One of the main goals of this paper is to analyze the semi-strong interaction reaction regime where the activator field concentrates on an arbitrary closed curve inside a 2-D domain $\Omega$. In this singularly perturbed limit, in §2 we derive a new moving boundary problem for (1.1), which characterizes the slow time evolution of the curve. This reduced problem is defined in terms of a quasi steady-state inhibitor diffusion field and its associated jump and continuity conditions across the curve. The formulation of this curve-evolution problem below in (2.13) differs substantially from that of the more traditional mean curvature flows and quasi-static moving boundary problems common in the field of materials science. As such, in the companion article [26], a new numerical methodology was developed to compute curve evolution from our quasi-static moving BVP. With this hybrid analytical-numerical approach to study localized pattern formation, the qualitatively interesting curve-evolution dynamics observed below in Fig. 2.1 for the GMS model provides an impetus to analyze the existence and stability of ring and near-ring solutions to the GMS model in radially symmetric geometries.

With this motivation, the main focus of the paper is to analyze the existence, stability, and dynamics of ring solutions to the GMS model with reaction kinetics (1.7) in radially symmetric domains. When saturation is not present, it was shown previously that steady-state ring solutions do not exist below a critical saddle-node fold bifurcation point (cf. [29]). This leads to a saddle-node bifurcation diagram for ring equilibria when there is no saturation. However, in §3 we show that the inclusion of saturation induces a change in the small radius ring dynamics, which creates a third steady-state ring radius. The corresponding bifurcation diagram for steady-state ring radii with saturation is S-shaped, thereby allowing for hysteretic transitions, and is such that steady-state ring solutions exist at all ring radii. This qualitatively new result due to saturation is possibly linked to the discussion in [34], where it was noted that patterns on a freshwater snail, *Theodoxus fluviatilis*, change drastically because of concentrations of salt in the water they are exposed to. A hysteresis-type bifurcation diagram provides a mechanism to allow for such drastic changes that cannot be described with a saddle-node bifurcation structure of steady-state solutions.

In §3 we then use our quasi-static moving BVP curve-evolution problem to study the effect of perturbations to the radially symmetric solution for a near-ring interface. We show that a two-term, and not simply a one-term, asymptotic expansion of this problem is essential to capture important qualitative information of the curve dynamics resulting from perturbations in the normal velocity. In particular, the leading-order term introduces the sinusoidal perturbation to the constant velocity that is due to the angular perturbation of the interface, while the second order term is needed to analyze the constant shift in the velocity, which induces a non-zero drift of the average interface location. For small ring radii we show analytically that non-radially symmetric initial perturbations of the ring will eventually stabilize, and lead to the circularization of the curve as time increases.

In §4 we use a WKB approach to formulate the linear stability problem for a ring solution in a radially symmetric domain. We show that the spectrum is divided into two classes of eigenvalues arising from either locally even or odd eigenfunctions across the ring, each of which are analyzed in §4.1 and §4.2, respectively. The breakup instability analysis resulting from locally even eigenfunctions relies on the derivation and analysis of a non-local eigenvalue problem (NLEP), the main conclusions of which mirror the analysis in [17] of a straight-stripe solution and, as such, are only briefly summarized. The main result of this analysis is that when the saturation parameter is sufficiently large there is no longer any breakup instability for a ring. The existence of such a stabilizing mechanism due to saturation has key implications for solutions of our reduced curve-evolution problem (2.13) since it implies that its computed solutions will persist as solutions to the full RD system.

In addition, in §4.2 we also analyze zig-zag instabilities of a ring solution, resulting from locally odd eigenfunctions near the curve, which can distort the shape of the curve. The analysis of these zig-zag instabilities for a ring is a new result, and does not follow in a straightforward manner from the corresponding analysis of zig-zag instabilities of a straight stripe solution done in [17]. As a result of the non-zero curvature of the ring, a rather delicate matched asymptotic expansion analysis is needed to derive a formula for the small eigenvalues of order $\mathcal{O}(\epsilon^2)$, which characterizes zig-zag instabilities. We also show, as expected intuitively, that these small eigenvalues are related to the first order velocity corrections of the near-circular ring problem. This is significant because it shows the bifurcation from radially symmetric solutions to solutions of near radial symmetry analyzed in §3. Therefore, in order that the moving BVP curve-evolution dynamics (2.13) accurately approximate solutions to the full RD system it is only essential to ensure that the ring solution is stable to locally even perturbations across the curve, as characterized by the spectrum of the NLEP.

In §5, we present full numerical results to demonstrate predicted breakup modes in the absence of saturation, as well as the stabilizing effect that saturation has on such patterns. We show the curve circularization tendency for perturbed circles of small radii, but also show that the curve can destabilize if made larger, or if the inhibitor diffusion coefficient is appropriately scaled. Finally, in §6, we briefly summarize our main results, and we suggest a few open problems that warrant further investigation.

**1.1. Boundary Fitted Coordinate Formulation.** Due to the singularly perturbed nature of the activator, we will construct a local boundary fitted coordinate system (cf. [11], [13]) $(x, y) \to (\eta, s)$ where $\eta$ is the signed normal distance from a curve (inward is positive) and $s$ is the curve arclength. In this coordinate frame, and sufficiently close to the curve,

$$\Delta = \partial_{\eta\eta} - \frac{\kappa}{(1-\kappa\eta)}\partial_\eta + \frac{1}{(1-\kappa\eta)}\partial_s\left(\frac{\partial_s}{(1-\kappa\eta)}\right), \tag{1.3}$$

where $\kappa$ is the signed curvature (positive for convex curves). We consider $g(u, v)$ from (1.1) such that $g(u, 0) = 0$ so by (1.1), the activator is identically zero except for a region of $\mathcal{O}(\epsilon)$ near the interface. With this in mind we introduce the following inner coordinate scaling:

$$\hat{\eta} = \frac{\eta}{\epsilon}; \qquad \tilde{v}(\hat{\eta}, s) = v(\epsilon\hat{\eta}, s), \quad \tilde{u}(\hat{\eta}, s) = u(\epsilon\hat{\eta}, s)\,. \tag{1.4}$$

Furthermore, we will construct quasi-steady solutions where the only dynamic component arises from the evolution of a front. Asymptotic balance requires that this curve dynamic time scale satisfies $T = \epsilon^2 t$. Using this time scale, we have that (1.1) transforms under the inner coordinate system to

$$\epsilon\dot{\eta}\tilde{v}_{\hat{\eta}} + \epsilon^2\dot{s}\tilde{v}_s = \tilde{\Delta}\tilde{v} - \tilde{v} + g(\tilde{u},\tilde{v}), \tag{1.5a}$$

$$\epsilon^3\tau\dot{\eta}\tilde{u}_{\hat{\eta}} + \epsilon^4\tau\dot{s}\tilde{u}_s = D\tilde{\Delta}\tilde{u} - \epsilon^2\tilde{u} + \epsilon f(\tilde{u},\tilde{v})\,, \tag{1.5b}$$

where $\dot{\eta}$ and $\dot{s}$ are the normal and arclength velocities, and the inner Laplace operator satisfies,

$$\tilde{\Delta} \equiv \partial_{\hat{\eta}\hat{\eta}} - \frac{\epsilon\kappa}{(1-\epsilon\kappa\hat{\eta})}\partial_{\hat{\eta}} + \frac{\epsilon^2}{(1-\epsilon\kappa\hat{\eta})}\partial_s\left(\frac{\partial_s}{(1-\epsilon\kappa\hat{\eta})}\right). \tag{1.6}$$

We will generalize results when possible for various $f(u,v)$ and $g(u,v)$ but will primarily focus on the saturated Gierer-Meinhardt (GMS) model (1.2) of the following form:

$$g(u,v) = \frac{v^2}{u^q(1+\sigma v^2)}, \qquad f(u,v) = \frac{v^o}{u^s}\,; \qquad qo-(s+1) > 0\,. \tag{1.7}$$

**2. The Singular Limit in the Semi-Strong Regime.** By expanding $u$ and $v$ in powers of $\epsilon$, we obtain from the leading order problem for (1.5) that $\tilde{u}_0 = U_0(s)$ and

$$\tilde{v}_{0\hat{\eta}\hat{\eta}} - \tilde{v}_0 + g(U_0,\tilde{v}_0) = 0\,; \qquad \tilde{v}_{0\hat{\eta}}(0) = 0, \qquad \lim_{|\hat{\eta}|\to\infty}\tilde{v}_0 = 0\,, \tag{2.1}$$

where the front-centering condition is imposed to eliminate translational invariance in the problem. We seek a homoclinic orbit solution of this problem that tends to the fixed point $\tilde{v}_0 = 0$ as $|\hat{\eta}| \to \infty$. A general result for the existence of such a homoclinic solution was first proved in Theorem 5 of [4] (see also [25]). The result is as follows:

Lemma 2.1. *Consider the problem of finding a $C^2$ smooth homoclinic orbit $w(y)$ on $-\infty < y < \infty$ satisfying*

$$w_{yy} - w + h(w) = 0\,, \qquad w \to 0 \quad as \quad |y| \to \infty; \qquad w'(0) = 0, \quad w_m = w(0) > 0\,, \tag{2.2}$$

*where we assume $h(w)$ is $C^1$ smooth on $w \geq 0$ with $h(0) = 0$ and $h'(0) < 1$. If we define $Q(w) \equiv h(w) - w$, so that $Q(0) = 0$ and $Q'(0) < 0$, and if*

1. *For $s > 0$, $Q(s) = 0$, $Q'(s) > 0$; $\quad Q(w) < 0$, for $0 < w < s$,*
2. *$Q(w) > 0$ for $s < w < w_m$ with $w_m$ satisfying $\int_0^{w_m} Q(w)\,\mathrm{d}w = 0$,*

*then a unique, positive, homoclinic orbit solution exists.*

Due to the structure of (2.1), the homoclinic orbit solution, if it exists, is necessarily even. In the context of the GMS model we identify that

$$w = \frac{\tilde{v}_0}{U_0^q}, \qquad h(w) = \frac{w^2}{(1+bw^2)}; \qquad \text{where} \qquad b \equiv U_0^{2q}\sigma > 0\,. \tag{2.3}$$

We now examine the conditions in Lemma 2.1 for this choice of nonlinearity. When $b \geq 1/4$ we observe that $Q(w) < 0$ for all $w \neq 0$ and therefore, condition 2 is not satisfied. Alternatively, for $b < 1/4$, $w = 0$ is a root together with the two additional roots

$$w^{\pm} = (1 \pm \sqrt{1-4b})/2b\,, \tag{2.4}$$

with $Q(w) < 0$ on $0 < w < w^-$ satisfying condition 1 of Lemma 2.1. Condition 2 is then satisfied for $w_m \leq w^+$ if

$$\int_{w^-}^{w^+} Q(w)\,\mathrm{d}w \geq \int_0^{w^-} |Q(w)|\,\mathrm{d}w\,. \tag{2.5}$$

This inequality will hold up until the value $b = b_c$ where $w_m = w^+(b_c)$ and therefore a homoclinic orbit exists when $0 \leq b < b_c$ with

$$b_c = 0.211376, \quad w_m(b_c) = 3.29521\,, \tag{2.6}$$

as was first reported in [17].

If we continue the activator-inhibitor expansion to $\mathcal{O}(\epsilon)$ then

$$L\tilde{v}_1 = \kappa\tilde{v}_{0\hat{\eta}} - g_u(U_0,\tilde{v}_0)\tilde{u}_1 + \tilde{v}_{0\hat{\eta}}\dot{\eta}\,, \qquad \tilde{u}_{1\hat{\eta}\hat{\eta}} = -\frac{1}{D}f(U_0,\tilde{v}_0)\,, \tag{2.7}$$

where $L\tilde{v}_1 \equiv \tilde{v}_{1\hat{\eta}\hat{\eta}} - \tilde{v}_1 + g_v(U_0,\tilde{v}_0)\tilde{v}_1$. By the translational invariance of (2.1) $\tilde{v}_1 = \tilde{v}_{0\hat{\eta}}$ is a homogeneous solution to (2.7) for $\tilde{v}_1$. This leads to the following solvability condition:

$$\dot{\eta} = -\kappa - \frac{1}{\int_{-\infty}^{\infty}\tilde{v}_{0\hat{\eta}}^2\,\mathrm{d}\hat{\eta}}\int_{-\infty}^{\infty}\mathcal{G}\tilde{u}_{1\hat{\eta}}\,\mathrm{d}\hat{\eta}; \qquad \mathcal{G} \equiv \int_0^{\tilde{v}_0} g_u(U_0,x)\,\mathrm{d}x\,. \tag{2.8}$$

Upon integrating this expression by parts, and using (2.7) for $\tilde{u}_1$, we get

$$\int_{-\infty}^{\infty}\mathcal{G}\tilde{u}_{1\hat{\eta}}\,\mathrm{d}\hat{\eta} = \hat{\mathcal{G}}\tilde{u}_{1\hat{\eta}}\Big|_{-\infty}^{\infty} + \frac{1}{D}\int_{-\infty}^{\infty}\hat{\mathcal{G}}f(U_0,\tilde{v}_0)\,\mathrm{d}\hat{\eta}\,; \qquad \hat{\mathcal{G}}(\hat{\eta}) \equiv \int_0^{\hat{\eta}}\mathcal{G}(x)\,\mathrm{d}x\,. \tag{2.9}$$

Finally, since $f(u,v)$ is an even function in $v$, while $\hat{\mathcal{G}}$ is odd, we obtain the front velocity condition that

$$\dot{\eta} = -\kappa - 2\mathcal{H}\left\langle\frac{\partial u}{\partial\eta}\right\rangle_{\eta=0}, \qquad \mathcal{H} \equiv \frac{\hat{\mathcal{G}}(+\infty)}{\int_{-\infty}^{\infty}\tilde{v}_{0\hat{\eta}}^2\,\mathrm{d}\hat{\eta}}\,, \tag{2.10}$$

where $\langle\cdot\rangle_{\eta=a}$ is the average across $\eta = a$ and we have used matching conditions to the outer region to rewrite the derivative. Moreover, by integrating (2.7) for $\tilde{u}_1$, we get

$$\left[\frac{\mathrm{d}u}{\mathrm{d}\eta}\right]_{\eta=0} = -\frac{1}{D}\int_{-\infty}^{\infty} f(U_0,\tilde{v}_0)\,\mathrm{d}\hat{\eta}\,, \tag{2.11}$$

where $[\cdot]_{\eta=a}$ indicates a jump across $\eta = a$.

Now consider the global problem where $\eta = \mathcal{O}(1)$ given by (1.1). Since $f(u,0) = 0$ and $v$ decays exponentially in the far-field, then to leading order

$$\lim_{\epsilon\to 0}\frac{f(u,v)}{\epsilon} = \left(\int_{-\infty}^{\infty} f(U_0,\tilde{v}_0)\,\mathrm{d}\hat{\eta}\right)\delta(\eta), \tag{2.12}$$

where $\delta(\cdot)$ is the Dirac measure. Integrating the equation for $u$ in (1.1) using this measure results precisely in the jump condition (2.11) as one would expect. Therefore, in the limit as

$\epsilon$ tends to zero, we can ignore the reaction term $f(u,v)$ in the global problem as long as we properly supplement with jump conditions on $u$. In this way, we have the following singular limit problem for the global inhibitor field:

Principal Result 2.1. *Consider an activator $v$ and inhibitor $u$ to (1.1) on a domain $\Omega$ in $\mathbb{R}^2$ with Neumann boundary conditions on $\partial\Omega$. Suppose that the activator $v$ is localized as $\epsilon \to 0$ (in the sense of homoclinic orbit solutions defined by Lemma 2.1) entirely on a set of (possibly disjoint) curves $\Gamma$. The effective global problem for the inhibitor, which defines the interface velocity, is*

$$D\Delta u - u = 0\,, \qquad x \in \Omega \setminus \Gamma\,; \qquad \frac{\partial u}{\partial n} = 0\,, \qquad x \in \partial\Omega\,, \tag{2.13a}$$

$$u = U_0(s)\,, \qquad x \in \Gamma\,, \tag{2.13b}$$

$$\left[\frac{\partial u}{\partial n}\right]_\Gamma = -\frac{1}{D}\int_{-\infty}^{\infty} f(U_0, \tilde{v}_0)\,\mathrm{d}\hat{\eta}, \qquad x \in \Gamma\,, \tag{2.13c}$$

$$V = \kappa + 2\mathcal{H}\left\langle \frac{\partial u}{\partial n}\right\rangle_\Gamma\,. \tag{2.13d}$$

*The normal velocity to the curve, as measured with respect to the origin, is $V = -\dot{\eta}$.*

We remark that only for the special case where the interface is a circular ring concentric within a disk-shaped domain, is it possible to readily verify that equilibria of the reduced dynamics (2.13d), corresponding to setting $V = 0$ on $\Gamma$, do in fact correspond to true radially symmetric steady-state solutions where the activator concentrates on a circular ring concentric within the disk. Such ring-type solutions are analyzed in detail in §3.

While analytic solutions using this formulation are not generally possible for arbitrary curves $\Gamma$, recently in the companion article [26], a numerical methodology has been designed to solve moving-boundary problems of the type (2.13). This class of problems is new, as compared to the well-known Cahn-Hilliard problems of material science, in the sense that the normal velocity depends on the average, rather than the difference, of the diffusive flux across the interface [26]. As such, a novel numerical framework was developed in [26] to treat (2.13). Some numerical examples of solutions obtained using this methodology of [26] are presented in Fig. 2.1, where it is seen that the RD system has a rich set of dynamics to be understood. For example, in both Fig. 2.1a and Fig. 2.1b we start with similar initial conditions with the main difference being the radius of the domain and base radius of the curve. However, in Fig. 2.1a the perturbed circle shrinks and circularizes, while in Fig. 2.1b it grows and distorts.

It is important to emphasize that Fig. 2.1 is a simulation of the reduced dynamics, characterized by the moving-boundary problem (2.13), and not the full PDE system (1.1). To determine whether the reduced slow dynamics does in fact capture long-time behavior of the full PDE system (1.1) we need to analyze the linear stability properties of the linearization of the full PDE system (1.1). This is done in §4 for the class of ring-type solutions. For these ring-type solutions we will show that weak zig-zag instabilities, associated with eigenvalues of $\mathcal{O}(\epsilon^2)$ in the linearization, have a direct correspondence to small amplitude shape-deforming instabilities of the ring pattern associated with the reduced dynamics (2.13). We will further show for ring-type solutions that there are parameter regimes where there are no $\mathcal{O}(1)$ time-scale breakup instabilities associated with the profile of the ring solution, as characterized by the spectrum of a nonlocal eigenvalue problem NLEP. As such, our analysis suggests

that there are parameter regimes where the reduced moving-boundary dynamics, which can be computed using the algorithm in [26], should accurately reflect corresponding long-time behavior in the full PDE system (1.1). In the remainder of this manuscript, we will primarily focus on the simple geometrical configuration of a ring-type solution for which the development of an analytical theory is tractable.

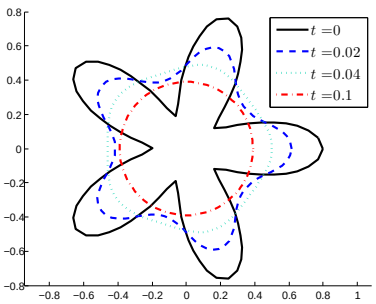


(a) $r_0 = 0.5 + 0.3\cos(5\theta)$

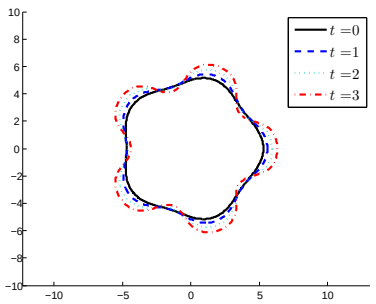


(b) $r_0 = 5 + 0.3\cos(5\theta)$

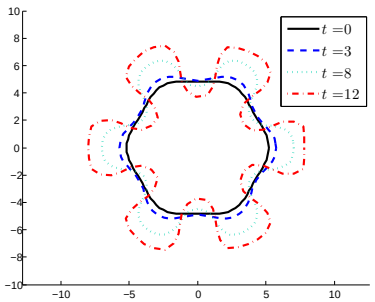


(c) $r_0 = 5 + 0.3\cos(6\theta)$

Figure 2.1: Some numerical solutions to (2.13) using the framework developed in [26]. For (a), we have taken the localized curve to be a near circle with radius given by $r_0 = 0.5+0.3\cos(5\theta)$ inside a larger circular domain $R = 1$. For (b), we have taken the localized curve to be a near circle with radius given by $r_0 = 5 + 0.3\cos(5\theta)$ inside a larger circular domain $R = 10$. The perturbation is identical to (a) but just with a larger curve base radius in a larger domain. For (c), we have taken $r_0 = 5+0.3\cos(6\theta)$ inside a larger circular domain $R = 10$. This curve grows and distorts even more than in (b). In all simulations we have chosen the exponent set $(2, q, o, s) = (2, 1, 2, 0)$, the saturation as $\sigma = 10$, and the diffusivity $D = 1$. We have omitted plotting the boundary of the domain $r = R$.

## 3. Ring and Near-Ring Solutions to the GMS Model.

In this section, we will explicitly consider the saturated Gierer-Meinhardt model where $f(u, v)$ and $g(u, v)$ in (2.13) are replaced with (1.7). First, we consider a ring solution where the activator is localized on a circle of

radius $r_0$ in a domain $0 < r < R$. For this geometry, we define the inner variable $\rho = (r - r_0)/\epsilon$. Upon solving (2.13) with a radially symmetric inhibitor field for this geometry we obtain the following result:

Principal Result 3.1. *For $\epsilon \to 0$ the quasi-equilibrium ring solution with radius $r_0$, satisfying $\mathcal{O}(\epsilon) \ll r_0 \ll 1 - \mathcal{O}(\epsilon)$, is given by*

$$v_e(r) \sim U_0^q w\left(\frac{r - r_0}{\epsilon}\right), \qquad u_e(r) \sim U_0 \frac{G_0(r; r_0)}{G_0(r_0; r_0)}, \tag{3.1}$$

*where $w$ is the homoclinic solution, as defined in Lemma 2.1, and $G_0$ is the Green's function that satisfies,*

$$G_{0rr} + \frac{1}{r} G_{0r} - \frac{1}{D} G_0 = -\delta(r - r_0); \quad 0 < r < R; \qquad G_{0r}(0) = G_{0r}(R) = 0. \tag{3.2}$$

*The solution to this problem for $G_0(r; r_0)$ is given by*

$$G_0(r; r_0) = \begin{cases} \mathcal{J}_{0,1}(r)\mathcal{J}_{0,2}(r_0), & 0 \le r \le r_0 \\ \mathcal{J}_{0,1}(r_0)\mathcal{J}_{0,2}(r), & r_0 \le r \le R \end{cases}, \tag{3.3}$$

$$\mathcal{J}_{0,1}(r) \equiv I_0\left(\frac{r}{\sqrt{D}}\right), \qquad \mathcal{J}_{0,2}(r) \equiv \alpha_0 I_0\left(\frac{r}{\sqrt{D}}\right) + K_0\left(\frac{r}{\sqrt{D}}\right), \qquad \alpha_0 \equiv \frac{K_1\left(\frac{R}{\sqrt{D}}\right)}{I_1\left(\frac{R}{\sqrt{D}}\right)}, \tag{3.4}$$

*where $I_n$ and $K_n$ are the modified Bessel functions of order $n$. The constant $U_0$ is determined by applying (2.13c), which yields*

$$U_0^{\beta - 1} = \frac{D}{r_0 \mathcal{A} G_0(r_0; r_0)}; \qquad \beta = qo - s, \qquad \mathcal{A} = \int_{-\infty}^{\infty} w^o \, \mathrm{d}\rho. \tag{3.5}$$

*When the parameter $b \neq 0$, as defined in (2.3), then this is an implicit expression for $U_0$ since $\mathcal{A}$ has a $U_0$ dependence. However, if we define*

$$\tilde{G}(b) \equiv b\mathcal{A}^{\frac{2q}{\beta - 1}} = \left(\frac{D}{r_0 G_0(r_0; r_0)}\right)^{\frac{2q}{\beta - 1}} \sigma, \tag{3.6}$$

*then we can conclude numerically that $d\mathcal{A}/db > 0$. Therefore, we have that $d\tilde{G}/db > 0$ so that for each $\sigma$ there is a unique $b$. When $o = 2$, this monotonicity property was shown to hold analytically in [43]. Finally, using (2.13d), the dynamic condition for the ring motion becomes*

$$\frac{\mathrm{d}r_0}{\mathrm{d}T} = -\frac{1}{r_0} - \frac{q}{4}\hat{\mathcal{H}}\left(\frac{\mathcal{J}_{0,1}'(r_0)}{\mathcal{J}_{0,1}(r_0)} + \frac{\mathcal{J}_{0,2}'(r_0)}{\mathcal{J}_{0,2}(r_0)}\right), \qquad \hat{\mathcal{H}} \equiv \frac{\int_{-\infty}^{\infty} w^2 \, \mathrm{d}\rho}{\int_{-\infty}^{\infty} w_\rho^2 \, \mathrm{d}\rho} - 1. \tag{3.7}$$

We emphasize that our construction of the quasi-equilibrium ring solution is asymptotically valid only when the ring radius satisfies $\mathcal{O}(\epsilon) \ll r_0 \ll 1 - \mathcal{O}(\epsilon)$. For the narrow range

where $r_0 = \mathcal{O}(\epsilon)$, a new type of localized solution for the GMS model exists in the form of a droplet, or bubble-type solution, similar to that constructed in [35] in the limit of large saturation. We do not consider such a droplet solution here.

We further remark that the expression for $\hat{\mathcal{H}}$, in (3.7) arises from evaluating (2.9) for the GMS model (1.7), and then using (2.2) to simplify the resulting expression. Typically one considers a scaling where the diffusivity is absorbed into the length scale ($R = 1/\sqrt{D} = \ell$) and so we will take $D = 1$ and $R = \ell$ to be varied. When saturation is neglected, the problem remains invariant under this transformation. However, when $\sigma \neq 0$, the invariance is broken since, for a given $b$ value, different saturation constants, $\sigma$, are needed for the problem of $D$ and $R$ variable than for $D = 1$ and $R$ variable. When $b = 0$, it has been shown (cf. [29]) that equilibrium values to (3.7) undergo a saddle-node bifurcation at some $R = R_c$ where there exists two equilibrium radii for $R > R_c$, with the larger radius yielding the stable equilibrium. The existence of a saddle-node bifurcation point when $\sigma = 0$ relies on $\hat{\mathcal{H}}$ being constant for all $r_0$. However, when $\sigma \neq 0$, then since $b = b(U_0)$ and $U_0$ depends on $r_0$, the value of $b$ depends on $r_0$ for a fixed saturation $\sigma$. Since the homoclinic orbit depends on $b$ then $\hat{\mathcal{H}}$ is no longer constant. We have the following lemma to describe the behaviour of $\hat{\mathcal{H}}$ for $r_0 \ll 1$ but with $r_0 \gg \mathcal{O}(\epsilon)$:

Lemma 3.1. *Consider (1.1) with $f(u, v)$ and $g(u, v)$ given by (1.7) and where the activator is localized on a ring of radius $r_0$ in a circular domain. Then, for $r_0 \ll 1$, but with $r_0 \gg \mathcal{O}(\epsilon)$, the dynamic condition (3.7) reduces to*

$$\frac{\mathrm{d}r_0}{\mathrm{d}T} \sim \left( \frac{q\hat{\mathcal{H}}}{4(\alpha_0 + \log(2) - \log(r_0) - \gamma)} - 1 \right) \frac{1}{r_0}\,, \tag{3.8}$$

*where $\gamma \approx 0.57722$ is the Euler-Mascheroni constant. If $\sigma = 0$ then we can compute the homoclinic orbit solution in Lemma 2.1 explicitly as $w = \frac{3}{2}\operatorname{sech}^2(\rho/2)$. In this case $\hat{\mathcal{H}} \equiv 4$ and by (3.8),*

$$\frac{\mathrm{d}r_0}{\mathrm{d}T} \sim -\frac{1}{r_0} \to -\infty\,. \tag{3.9}$$

*If $\sigma \neq 0$ then, when a homoclinic orbit exists by Lemma 2.1, it is a function of $r_0$ and specifically as $r_0 \to 0$, but with $r_0 \gg \mathcal{O}(\epsilon)$, it follows from (3.6) that $\mathcal{A}$ tends to infinity and so $b$ must tend to the critical parameter $b_c$. Therefore $\hat{\mathcal{H}}$ tends to infinity in such a way that by (3.8), we have $\frac{\mathrm{d}r_0}{\mathrm{d}T} \to +\infty$ on the regime where $\mathcal{O}(\epsilon) \ll r_0 \ll 1$.*

The introduction of saturation has quite a drastic effect on the limiting behaviour of (3.8). To investigate this we consider a small, non-zero saturation such that $\sigma \ll 1$. For $r_0 \sim \mathcal{O}(1)$, (3.6) implies that $b \sim \sigma \ll 1$ and we expect that the leading order ($b = 0$) behaviour persists. However, consider scaling $r_0 = \sigma^x R_0$ for some $x > 0$ so that in (3.6) we have

$$\tilde{G}(b) \approx \nu \left( \frac{D}{R_0} \right)^{\zeta}; \qquad \nu = \sigma^{1-\zeta x} \log(\sigma^{-x})^{-\zeta}\,, \quad \zeta \equiv \frac{2q}{\beta - 1}\,, \tag{3.10}$$

where we have taken $G_0 \sim \log(\sigma^{-x})$ for $\sigma \ll 1$. However, $\tilde{G}(b) = b\mathcal{A}^{\zeta}$ as well and since $\tilde{G}$ is monotonic in $b$ then there must be a value of $b$ for all values of $\sigma$ regardless of $r_0$. This value

of $b$ must satisfy $0 \leq b \leq b_c$ and therefore since $\nu \gg 1$ then $A \sim \nu^{1/\zeta}$. It is reasonable to expect that this will also be the scaling for $\hat{\mathcal{H}}$ as defined in (3.7) and therefore from (3.8),

$$\frac{q\hat{\mathcal{H}}}{4(\alpha_0 + \log(2) - \log(\sigma^x R_0) - \gamma)} \sim \frac{\nu}{\log(\sigma^{-x})} = \frac{\sigma^{\frac{1-\zeta x}{\zeta}}}{\log(\sigma^{-x})^2} = \omega\,. \tag{3.11}$$

For $x$ not too large then $\omega \ll 1$ and the leading order behaviour in (3.8), $\frac{\mathrm{d}r_0}{\mathrm{d}T} \to -\infty$ persists as when $\sigma = 0$. However, as $r_0$ gets smaller and $x$ increases then $\omega \gg 1$ and instead $\frac{\mathrm{d}r_0}{\mathrm{d}T} \to \infty$. To find the parameter $x$ where small to large behaviour transitions we look for the roots $\omega = 1$ of which there are two, $x^-$ and $x^+$. However, we also require that $\nu \gg 1$ when $\omega \gg 1$ and so we take $x = x^+$ as the transition point above which $\omega \gg 1$. To support this discussion we plot $b$ versus $r_0$ in Fig. 3.1 for various values of the saturation parameter $\sigma$. Indeed we see that for $\sigma \ll 1$ and $r_0$ not too small that $b \approx 0$ as we expected. We also observe the boundary layer behaviour as $r_0$ tends to zero. For $\sigma \gg 1$, $b$ is equal to the saturation value for a large range of $r_0$. This could be expected once again by considering $\tilde{G}(b)$ in (3.6) where now $\sigma \gg 1$ and therefore $\mathcal{A} \gg 1$ unless $r_0$ is sufficiently large. To generate Fig. 3.1 we solved (3.6) for $b$ using Newton's method for a fixed value of $\sigma$ and by varying $r_0$. In Fig. 3.2, we plot $\frac{\mathrm{d}r_0}{\mathrm{d}T}$ for various values of $R = \ell$ in the cases of no saturation (left figure) and when $\sigma = 0.5$ (right figure). We once again observe that, aside from $r_0 \ll 1$, the small saturation causes a negligible deviation from $b = 0$.

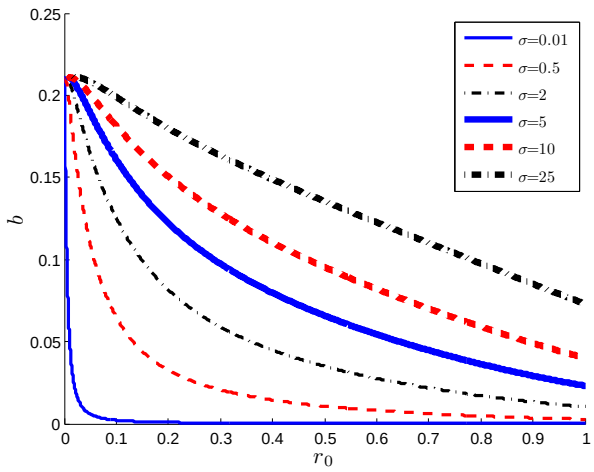


Figure 3.1: Modified saturation parameter $b$ as a function of $r_0$ for various saturation values $\sigma$. Here we take $D = 1$, $R = 1$ and the exponent set $(2, 1, 2, 0)$.

The $r_0 \ll 1$ boundary layer has quite a significant role on the overall structure of the equilibrium solutions. For the case of no saturation, Fig. 3.2a shows the existence of the saddle-node bifurcation in that no equilibrium values exist until a critical $R = R_c = 3.622$. However, with saturation, we obtain the qualitatively new result, as seen in Fig. 3.2b, that

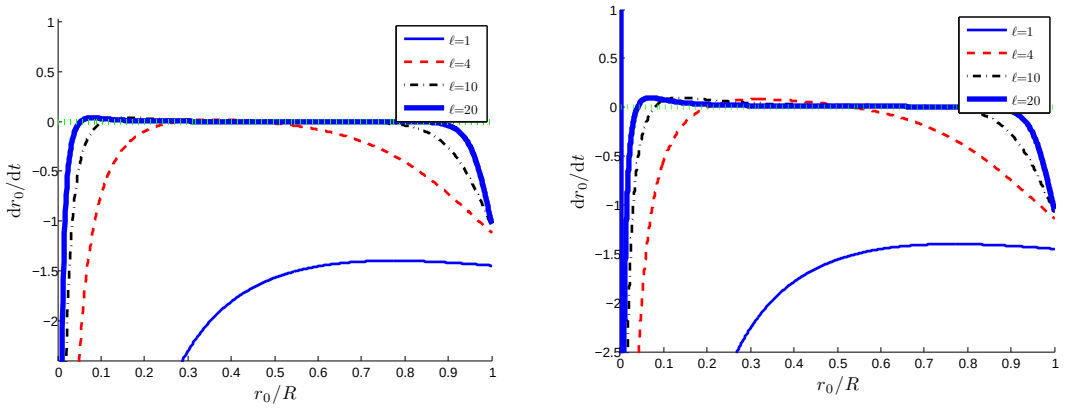


(a) $\sigma = 0$ (b) $\sigma = 0.5$

Figure 3.2: Right-hand side of (3.7) for various domain radii $R = \ell$. The exponent set is $(2, 1, 2, 0)$ and $D = 1$.

a new small equilibrium radius exists for all $R$ due to the limiting $r_0$ behaviour when $\sigma \neq 0$ in Lemma 3.1. Therefore, adding saturation allows a new branch of equilibrium solutions to emerge from $r_0 = 0$. Overall, the effect of the saturation parameter is that the saddle-node bifurcation diagram for $\sigma = 0$ characterizing equilibria of the ring dynamics is deformed into an $S$-shaped bifurcation diagram, which now allows for hysteresis behavior. Fig. 3.3 demonstrates this for $\sigma = 8$.

**3.1. Near-Ring Solutions.** Next, we consider near-ring solutions to the GMS model. By a near-ring we mean localizing the activator on a curve with radial perturbation $r = r_0 + \varepsilon h(\theta)$ for $\varepsilon \ll 1$ and $h(\theta)$ to be some smooth periodic function. The immediate advantage of the singular limit formulation (2.13) is evident here as this formulation is as amendable to this new problem as it was to the ring. For asymptotic consistency, we require that $\varepsilon \gg \epsilon$ so that the singular limit problem at $\mathcal{O}(1)$ is still valid.

To analyze the near-ring behavior we make a formal expansion of the inhibitor field as

$$u(r, \theta) = u_0(r) + \varepsilon u_1(r, \theta) + \varepsilon^2 u_2(r, \theta) + \dots , \tag{3.12}$$

where we explicitly note that we want to consider a perturbation from the radially symmetric inhibitor solution. Upon using this expansion, we have that the curve value $U_0$ and normal

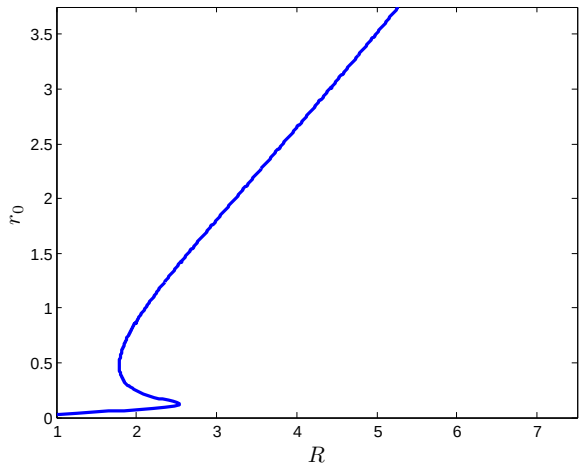


Figure 3.3: Bifurcation diagram for equilibria of (3.7) for $\sigma = 8$, $D = 1$, and exponent set $(2, 1, 2, 0)$.

derivative can be expanded as

$$\begin{aligned} U_0 = u(r_0 + \varepsilon h(\theta)) &\sim u_0(r_0) + \varepsilon(u_{0r}(r)h(\theta) + u_1(r))_{r_0} \\ &\quad + \varepsilon^2 \left( \frac{1}{2} u_{0rr}(r)[h(\theta)]^2 + u_{1r}(r)h(\theta) + u_2(r) \right)_{r_0} \\ &= U_{00} + \varepsilon U_{01}(\theta) + \varepsilon^2 U_{02}(\theta)\,, \qquad (3.13a) \\ \left.\frac{\mathrm{d}u}{\mathrm{d}n}\right|_{r=r_0^\pm} &\sim -u_{0r}(r_0^\pm) + \varepsilon \left( -u_{0rr}(r_0^\pm)h(\theta) - u_{1r}(r_0^\pm) \right) \\ &\quad + \varepsilon^2 \left( -\frac{1}{2} u_{0rrr}(r_0^\pm)[h(\theta)]^2 - u_{1rr}(r_0^\pm)h(\theta) + \frac{u_{1\theta}(r_0^\pm)h'(\theta)}{r_0^2} \right. \\ &\quad \left. + \frac{u_{0r}(r_0^\pm)[h'(\theta)]^2}{2r_0^2} - u_{2r}(r_0^\pm) \right)\,. \qquad (3.13b) \end{aligned}$$

The notation $(\cdot)_{r_0}$ indicates an evaluation at $r = r_0$ and we do this externally because individual terms may be discontinuous but they must combine to form a continuous curve value. In the presence of saturation, we must also consider expansions similar to (3.12) for $\mathcal{A}$, $\hat{\mathcal{H}}$, and $b$ given by (3.5), (3.7), and (2.3) respectively. The leading order solution $u_0$ is the radially symmetric inhibitor problem on a ring, which was defined in Principal Result 3.1. Using

(3.13), the problem at $\mathcal{O}(\varepsilon)$ for $u_1$ is

$$\frac{1}{r}\frac{\partial}{\partial r}\left(r\frac{\partial u_1}{\partial r}\right)+\frac{1}{r^2}\frac{\partial^2 u_1}{\partial \theta^2}-\frac{1}{D}u_1=0\,,\qquad r\neq r_0\,,\qquad \left.\frac{\partial u_1}{\partial r}\right|_{r=R}=0\,, \tag{3.14a}$$

$$[u_1]_{r_0}=-h(\theta)\left[\frac{\mathrm{d}u_0}{\mathrm{d}r}\right]_{r_0}\,, \tag{3.14b}$$

$$\left[\frac{\partial u_1}{\partial r}\right]_{r_0}=-h(\theta)\left[\frac{\mathrm{d}^2u_0}{\mathrm{d}r^2}\right]_{r_0}-\frac{\bar{A}_0}{U_{00}}\bar{\bar{A}}_0U_{01}\,, \tag{3.14c}$$

where we have defined

$$\bar{A}_0\equiv\frac{\mathcal{A}_0}{D}U_{00}^{\beta}=\frac{U_{00}}{r_0G_0(r_0;r_0)}\,,\qquad \bar{\bar{A}}_0\equiv\beta+\frac{2qb_0}{\mathcal{A}_0}\frac{\mathrm{d}\mathcal{A}_0}{\mathrm{d}b}\,. \tag{3.15}$$

The zero subscripts indicate evaluations of saturation dependent functions at the constant value $U_{00}$. To calculate the terms in this expression involving $u_0$, we use the standard Wronskian relation

$$W_{0,n}(r)\equiv I_n\left(\frac{r}{\sqrt{D}}\right)\frac{\mathrm{d}}{\mathrm{d}r}K_n\left(\frac{r}{\sqrt{D}}\right)-K_n\left(\frac{r}{\sqrt{D}}\right)\frac{\mathrm{d}}{\mathrm{d}r}I_n\left(\frac{r}{\sqrt{D}}\right)=-\frac{1}{r}\,. \tag{3.16}$$

In this way, we can rewrite (3.14b) and (3.14c) as

$$[u_1]_{r_0}=h(\theta)\bar{A}_0\,,\qquad \left[\frac{\partial u_1}{\partial r}\right]_{r_0}=-h(\theta)\frac{\bar{A}_0}{r_0}-\frac{\bar{A}_0}{U_{00}}\bar{\bar{A}}_0U_{01}\,. \tag{3.17}$$

We then introduce the Fourier eigenfunction expansion

$$u_1(r,\theta)=\sum_{n=-\infty}^{\infty}\mathcal{V}_{1n}(r)\exp(in\theta)\,,\quad U_{01}(\theta)=\sum_{n=-\infty}^{\infty}\mathcal{U}_{1n}\exp(in\theta)\,,\quad h(\theta)=\sum_{n=-\infty}^{\infty}H_n\exp(in\theta)\,, \tag{3.18}$$

which leads to the following result regarding the solution to (3.14):

Principal Result 3.2. *In terms of the Fourier decomposition (3.18), the solution to (3.14), with (3.17), is*

$$\mathcal{V}_{1n}(r)=\bar{A}_{1n}r_0G_{1,n}(r;r_0)-\bar{B}_{1n}r_0G_{0,n}(r;r_0)\,, \tag{3.19}$$

*with constants $\bar{A}_{1n}$ and $\bar{B}_{1n}$ defined by*

$$\bar{A}_{1n}\equiv H_n\bar{A}_0\,,\qquad \bar{B}_{1n}\equiv-\frac{H_n\bar{A}_0}{r_0}-\frac{\bar{A}_0}{U_{00}}\bar{\bar{A}}_0\mathcal{U}_{1n}\,. \tag{3.20}$$

*Here we have defined the Green's functions $G_{0,n}$ and $G_{1,n}$ as*

$$G_{0,n}(r;r_0)\equiv\begin{cases}\mathcal{J}_{n,1}(r)\mathcal{J}_{n,2}(r_0), & 0\le r\le r_0\\ \mathcal{J}_{n,1}(r_0)\mathcal{J}_{n,2}(r), & r_0\le r\le R\end{cases}\,,\quad G_{1,n}(r;r_0)\equiv\begin{cases}\mathcal{J}_{n,1}(r)\mathcal{J}'_{n,2}(r_0), & 0\le r<r_0\\ \mathcal{J}'_{n,1}(r_0)\mathcal{J}_{n,2}(r), & r_0<r\le R\end{cases}\,, \tag{3.21}$$

*with $\mathcal{J}_{n,i}(r)$ defined similarly as in (3.4). We note that $G_{1,n}$ is not continuous across $r = r_0$ as is expected by the jump condition (3.14b). Using (3.13a), we have that*

$$\mathcal{U}_{1n} = \left( \mathcal{V}_{1n} + H_n \frac{\mathrm{d}u_0}{\mathrm{d}r} \right)_{r_0} . \tag{3.22}$$

*Although each of the two terms in this expression are discontinuous across $r = r_0$, we have that $\mathcal{U}_{1n}$ is continuous, and so $\mathcal{U}_{1n} = \langle \mathcal{U}_{1n} \rangle_{r=r_0}$. By explicitly evaluating the terms in this expression we obtain that*

$$\mathcal{U}_{1n} = \frac{H_n U_{00}}{G_0(r_0;r_0)} \left( 1 - \bar{\bar{A}}_0 \frac{G_{0;n}(r_0;r_0)}{G_0(r_0;r_0)} \right)^{-1} \left( \frac{G_{0,n}(r_0;r_0)}{r_0} + \left\langle G_{1,n}(r,r_0) + \frac{\mathrm{d}G_0}{\mathrm{d}r} \right\rangle_{r_0} \right) . \tag{3.23}$$

*Furthermore, the unsigned curvature at $\mathcal{O}(\varepsilon)$ is*

$$\kappa_1 = r_0^{-2} \left[ h''(\theta) + h(\theta) \right] , \tag{3.24}$$

*and, therefore, by expanding (2.13d) to $\mathcal{O}(\varepsilon)$, we generate a perturbed interface velocity $V_{01}$ of the form*

$$V_{01} = -\kappa_1 - \frac{q\hat{\mathcal{H}}_0}{2U_{00}^2} \left( 1 - \frac{2qb_0}{\hat{\mathcal{H}}_0} \frac{\mathrm{d}\hat{\mathcal{H}}_0}{\mathrm{d}b} \right) \left\langle \frac{\mathrm{d}u_0}{\mathrm{d}r} \right\rangle_{r_0} U_{01} + \frac{q\hat{\mathcal{H}}_0}{2U_{00}} \left( h(\theta) \left\langle \frac{\mathrm{d}^2 u_0}{\mathrm{d}r^2} \right\rangle_{r_0} + \left\langle \frac{\partial u_1}{\partial r} \right\rangle_{r_0} \right) . \tag{3.25}$$

*Here $\hat{\mathcal{H}}$ is defined in (3.7), while $u_1$ and $U_{01}$ are given in (3.18).*

From (3.25) we obtain that the velocity perturbation has the limiting behavior $V_{01} \sim -\kappa_1$ for $r_0 \ll 1$. As such, for typical perturbations of the form $h(\theta) = \cos(m\theta)$, the interface velocity is in phase with $h(\theta)$ and will circularize the curve. This was evidenced in Fig. 2.1 where our choice $r_0 = 0.5$ lead to an overall circularization of a perturbed curve. However for larger values of $r_0$, the curve grew and distorted from a circle. Overall then, (3.25) show that curves of low curvature can grow because of radial gradients in the steady-state. Immediately we see from Principal Result 3.2 that introducing sinusoidal perturbations induces contributions of each perturbed mode to the inhibitor solution. However, any modes, aside from $n = 0$, cannot describe vertical shifting from the unperturbed value $U_{00}$ and as such, we must consider second-order perturbations at $\mathcal{O}(\varepsilon^2)$.

At $\mathcal{O}(\varepsilon^2)$ the base problem is the same as (3.14), but is now subject to the new jump conditions

$$[u_2]_{r_0} = -h(\theta) \left[ \frac{\partial u_1}{\partial r} \right]_{r_0} - \frac{[h(\theta)]^2}{2} \left[ \frac{\mathrm{d}^2 u_0}{\mathrm{d}r^2} \right]_{r_0} , \tag{3.26a}$$

$$\left[ \frac{\partial u_2}{\partial r} \right]_{r_0} = \frac{1}{2} \frac{[h'(\theta)]^2}{r_0^2} \left[ \frac{\mathrm{d}u_0}{\mathrm{d}r} \right]_{r_0} + \frac{h'(\theta)}{r_0^2} \left[ \frac{\partial u_1}{\partial \theta} \right]_{r_0} - h(\theta) \left[ \frac{\partial^2 u_1}{\partial r^2} \right]_{r_0} - \frac{1}{2} [h(\theta)]^2 \left[ \frac{\mathrm{d}^3 u_0}{\mathrm{d}r^3} \right]_{r_0} - \frac{\bar{A}_0}{U_{00}^2} \left( \bar{\bar{A}}_1 U_{01}^2 + \bar{\bar{A}}_0 U_{00} U_{02} \right) , \tag{3.26b}$$

with

$$\bar{\bar{A}}_1 = \frac{1}{2}\beta(\beta-1) + \frac{qb_0(2q-1)}{A_0}\frac{\mathrm{d}A_0}{\mathrm{d}b} + \frac{2q^2b_0^2}{A_0}\frac{\mathrm{d}^2A_0}{\mathrm{d}b^2}\,. \tag{3.27}$$

Using (3.17) for (3.26a), together with (3.18) and Principal Result 3.2, we calculate that

$$[u_2]_{r_0} = [h(\theta)]^2\frac{\bar{A}_0}{2r_0} + h(\theta)\frac{\bar{A}_0\bar{\bar{A}}_0}{U_{00}}U_{01}\,, \qquad \left[\frac{\partial u_1}{\partial\theta}\right]_{r_0} = \bar{A}_0h'(\theta)\,. \tag{3.28}$$

Then, upon using the Wronskian relationship defined by (3.16), together with the one defined by

$$W_{1,n}(r) \equiv \frac{\mathrm{d}}{\mathrm{d}r}I_n\left(\frac{r}{\sqrt{D}}\right)\frac{\mathrm{d}^2}{\mathrm{d}r^2}K_n\left(\frac{r}{\sqrt{D}}\right) - \frac{\mathrm{d}}{\mathrm{d}r}K_n\left(\frac{r}{\sqrt{D}}\right)\frac{\mathrm{d}^2}{\mathrm{d}r^2}I_n\left(\frac{r}{\sqrt{D}}\right) = \frac{n^2}{r^3} + \frac{1}{Dr}\,, \tag{3.29}$$

we have that

$$\left[\frac{\partial^2u_1}{\partial r^2}\right]_{r_0} = \sum_{n=-\infty}^{\infty}\left(\bar{A}_{1n}\left(\frac{n^2}{r^2}+\frac{1}{D}\right) - \frac{\bar{B}_{1n}}{r_0}\right)\exp(in\theta)\,, \tag{3.30a}$$

$$\left[\frac{\mathrm{d}^3u_0}{\mathrm{d}r^3}\right]_{r_0} = -\bar{A}_0\left(\frac{2}{r_0^2}+\frac{1}{D}\right)\,. \tag{3.30b}$$

Then, by using (3.18), we can simplify (3.30a) to

$$\left[\frac{\partial^2u_1}{\partial r^2}\right]_{r_0} = \frac{\bar{A}_0}{r_0^2}\left(h(\theta)-h''(\theta)\right) + \frac{\bar{A}_0}{D}h(\theta) + \frac{\bar{A}_0\bar{\bar{A}}_0}{U_{00}r_0}U_{01}\,. \tag{3.31}$$

Combining this expression with (3.28) and (3.30), we obtain that (3.26b) simplifies to

$$\left[\frac{\partial u_2}{\partial r}\right]_{r_0} = \frac{\bar{A}_0[h'(\theta)]^2}{2r_0^2} + \frac{\bar{A}_0}{r_0^2}h(\theta)h''(\theta) - \frac{\bar{A}_0}{2D}[h(\theta)]^2 - \frac{\bar{A}_0\bar{\bar{A}}_0}{U_{00}r_0}h(\theta)U_{01} - \frac{\bar{A}_0}{U_{00}^2}\left(\bar{\bar{A}}_1U_{01}^2 + \bar{\bar{A}}_0U_{00}U_{02}\right)\,. \tag{3.32}$$

Next, in order to analyze the solution to this problem for $u_2$ using an eigenfunction expansion, we need to treat products of infinite sums in a delicate way. Specifically, we will assume that the perturbations $h(\theta)$ are such that their Fourier series terminate, i.e. they are composed of a finite set of modes. This leads to the following definition:

Definition 3.2. *Assume two functions $f(\theta)$ and $g(\theta)$ have a Fourier series given by*

$$f(\theta) \sim \sum_{n=-\infty}^{\infty} a_n\exp(in\theta)\,, \qquad g(\theta) \sim \sum_{m=-\infty}^{\infty} b_m\exp(im\theta)\,,$$

*and that there exists some $N$ and $M$ such that $|a_n| = 0$ when $|n| > N$ and $|b_m| = 0$ when $|m| > M$. If this is the case then we can define the product of these functions as*

$$f(\theta)g(\theta) = \sum_{m=-\infty}^{\infty}\sum_{n=-\infty}^{\infty} a_nb_m\exp(i(n+m)\theta)\,.$$

This definition allows us to use the finite series product for handling the infinite sums which is in contrast to the Cauchy-product typically used. Using Definition 3.2 allows us express the inhibitor solution at $\mathcal{O}(\varepsilon^2)$ as a series expansion

$$u_2(r,\theta) = \sum_{k=-\infty}^{\infty} \mathcal{V}_{2k}(r)\exp(ik\theta)\,, \qquad U_{02}(\theta) = \sum_{k=-\infty}^{\infty} \mathcal{U}_{2k}\exp(ik\theta)\,, \tag{3.33}$$

which leads to the following result for the solution:

Principal Result 3.3. *Consider a series solution to (3.14) given by (3.33) with jump conditions (3.28) and (3.32) in place of (3.14b) and (3.14c) respectively. Only modes $k$ which exist as products of modes $n$ at $\mathcal{O}(\varepsilon)$ will produce non-zero components. As such, there exists a set $N_k$ for each valid $k$ containing the integer modes $n$ that produce mode $k$. Using this notation, we rewrite the jump conditions (3.28) and (3.32) as*

$$[\mathcal{V}_{2k}]_{r_0} = \frac{\bar{A}_0}{2r_0}\sum_{n\in N_k} H_n H_{k-n} + \frac{\bar{A}_0\bar{\bar{A}}_0}{U_{00}}\sum_{n\in N_k} H_n\mathcal{U}_{1k-n} \equiv \bar{A}_{2k}\,, \tag{3.34a}$$

$$\begin{aligned}\left[\frac{\mathrm{d}\mathcal{V}_{2k}}{\mathrm{d}r}\right]_{r_0} =& -\frac{\bar{A}_0}{2r_0^2}\sum_{n\in N_k} n(k-n)H_nH_{k-n} - \frac{\bar{A}_0}{r_0^2}\sum_{n\in N_k}(k-n)^2 H_nH_{k-n}\\ &- \frac{\bar{A}_0}{2D}\sum_{n\in N_k} H_nH_{k-n} - \frac{\bar{A}_0\bar{\bar{A}}_0}{U_{00}r_0}\sum_{n\in N_k} H_n\mathcal{U}_{1k-n}\\ &- \frac{\bar{A}_0}{U_{00}^2}\left(\bar{\bar{A}}_1\sum_{n\in N_k}\mathcal{U}_{1n}\mathcal{U}_{1k-n} + \bar{\bar{A}}_0U_{00}\mathcal{U}_{2k}\right) \equiv \bar{B}_{2k}\,.\end{aligned} \tag{3.34b}$$

*With the jump conditions defined in this way, the solution $\mathcal{V}_{2k}$ is decomposed as*

$$\mathcal{V}_{2k}(r) = \bar{A}_{2k}r_0G_{1,k}(r;r_0) - \bar{B}_{2k}r_0G_{0,k}(r;r_0)\,, \tag{3.35}$$

*where $G_{0,k}$ and $G_{1,k}$ are defined by (3.21). Using (3.13a), we have that*

$$\mathcal{U}_{2k} = \left(\frac{1}{2}\frac{\mathrm{d}^2u_0}{\mathrm{d}r^2}\sum_{n\in N_k} H_nH_{k-n} + \sum_{n\in N_k} H_n\frac{\mathrm{d}}{\mathrm{d}r}\mathcal{V}_{1k-n} + \mathcal{V}_{2k}\right)_{r_0}\,, \tag{3.36}$$

*which we can once again compute by taking the average to yield*

$$\begin{aligned}\mathcal{U}_{2k} =& \left(1 - \bar{\bar{A}}_0\frac{G_{0,k}(r_0;r_0)}{G_0(r_0;r_0)}\right)^{-1}\left(\frac{\bar{A}_0r_0}{2}\left\langle\frac{\mathrm{d}^2G_0}{\mathrm{d}r^2}\right\rangle_{r_0}\sum_{n\in N} H_nH_{k-n}\right.\\ &+r_0\sum_{n\in N}H_n\left(\bar{A}_{1k-n}\left\langle\frac{\mathrm{d}G_{1,k-n}}{\mathrm{d}r}\right\rangle_{r_0} - \bar{B}_{1k-n}\left\langle\frac{\mathrm{d}G_{0,k-n}}{\mathrm{d}r}\right\rangle_{r_0}\right)\\ &\left.+r_0\bar{A}_{2k}\left\langle G_{1,k}\right\rangle_{r_0} - r_0\tilde{B}_{2k}G_{0,k}(r_0;r_0)\right)\,,\end{aligned} \tag{3.37}$$

*where* $\tilde{B}_{2k} = \bar{B}_{2k} + \frac{\bar{A}_0 \bar{\bar{A}}_0}{U_{00}} \mathcal{U}_{2k}$. *Furthermore, the unsigned curvature at* $\mathcal{O}(\varepsilon^2)$ *is*

$$\kappa_2 = \frac{4h(\theta)h''(\theta) + [h'(\theta)]^2 + 2[h(\theta)]^2}{2r_0^3}\,. \tag{3.38}$$

*Therefore, expanding (2.13d) to* $\mathcal{O}(\varepsilon^2)$ *generates a velocity perturbation* $V_{02}$ *such that*

$$\begin{aligned} V_{02} =& \kappa_2 + \frac{q}{2}\left(\left(\frac{U_{01}^2}{U_{00}^2} - \frac{U_{02}}{U_{00}^2}\right)\hat{\mathcal{H}}_0 - \frac{U_{01}}{U_{00}^2}\frac{\mathrm{d}\hat{\mathcal{H}}_0}{\mathrm{d}b}b_1 \right. \\ &\left. + \frac{1}{U_{00}}\left(\frac{1}{2}\frac{\mathrm{d}^2\hat{\mathcal{H}}_0}{\mathrm{d}b^2}b_1^2 + \frac{\mathrm{d}\hat{\mathcal{H}}_0}{\mathrm{d}b}b_2\right)\right)\left\langle \frac{\mathrm{d}u_0}{\mathrm{d}r}\right\rangle_{r_0} + \frac{q}{2U_{00}^2}\left(U_{00}\frac{\mathrm{d}\hat{\mathcal{H}}_0}{\mathrm{d}b}b_1 - U_{01}\hat{\mathcal{H}}_0\right) \\ &\left(h(\theta)\left\langle \frac{\mathrm{d}^2u_0}{\mathrm{d}r^2}\right\rangle_{r_0} + \left\langle \frac{\partial u_1}{\partial r}\right\rangle_{r_0}\right) - \frac{q\hat{\mathcal{H}}_0}{2U_{00}}\left(-\frac{1}{2}[h(\theta)]^2\left\langle \frac{\mathrm{d}^3u_0}{\mathrm{d}r^3}\right\rangle_{r_0}\right. \\ &\left. -h(\theta)\left\langle \frac{\partial^2 u_1}{\partial r^2}\right\rangle_{r_0} + \frac{h'(\theta)}{r_0^2}\left\langle \frac{\partial u_1}{\partial \theta}\right\rangle_{r_0} + \frac{[h'(\theta)]^2}{2r_0^2}\left\langle \frac{\mathrm{d}u_0}{\mathrm{d}r}\right\rangle_{r_0} - \left\langle \frac{\partial^2 u_2}{\partial r^2}\right\rangle_{r_0}\right)\,, \end{aligned} \tag{3.39}$$

*where we have defined* $b_1$ *and* $b_2$ *as*

$$b_1 \equiv 2qU_{00}^{2q-1}U_{01}\sigma, \quad b_2 \equiv qU_{00}^{2q-2}\left((2q-1)U_{01}^2 + 2U_{00}U_{02}\right)\sigma\,. \tag{3.40}$$

To illustrate the summing set $N_k$, suppose that $h(\theta) = \cos(6\theta)$. There are two modes at $\mathcal{O}(\varepsilon)$ of $n = -6$ and $n = 6$. Various quadratic combinations of these modes leads to $k = -12$, $k = 0$, and $k = 12$ as the only possible modes that can occur at $\mathcal{O}(\varepsilon^2)$. Therefore, if $k = -12$ then $N_{-12} = \{-6\}$, while for $k = 0$ then the set is $N_0 = \{-6, 6\}$.

We can confirm Principal Results 3.2 and 3.3 by comparing to a numerically computed solution. The numerical solutions are generated from the framework derived in [26] and discussed in §2. We perform such simulations with $\sigma = 10$, $R = 1$, $D = 1$, exponent set $(2, 1, 2, 0)$, and $r_0 = 0.5$ with perturbation $h(\theta) = \cos(6\theta)$ and $\varepsilon = 0.01$. Fig. 3.4 shows the corrections at each order of $\varepsilon$ for $U_0$ and modified saturation parameter $b$, while Fig. 3.5 shows the corrections at each order of $\varepsilon$ for the velocity, $V$. The asymptotically predicted corrections of Principal Results 3.2 agree favourably and indeed demonstrate the need for both expansions to see the introduction of sinusoidal perturbations and the vertical shifts that are induced at $\mathcal{O}(\varepsilon^2)$.

**4. Linear Stability of the Ring Solution.** The numerical methodology in [26] generates numerical solutions to (2.13) but does not address the question of the linear stability of interface solutions to the RD system to any transverse perturbations. In particular, it has been shown for stripe solutions (cf. [17]), and for ring solutions with a particular exponent set (cf. [25]), that a certain class of eigenfunctions can lead to breakup instabilities for which the numerical solutions to (2.13) no longer characterize the slow dynamics of an interface. As such, it is important to investigate when instabilities of this nature could arise. For the stability analysis, we explicitly consider the base solution $v_e$ and $u_e$ to be asymptotically given

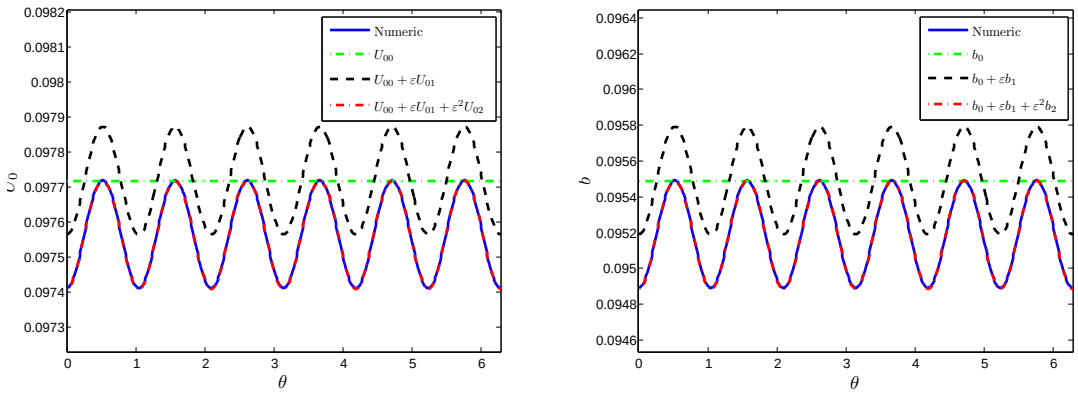


(a) $U_0$ corrections (b) $b$ corrections

Figure 3.4: Asymptotic corrections compared to full numerical simulations of the curve inhibitor value $U_0$ and the corresponding saturation value $b$ from solving (2.13) for a perturbed circle with radius $r = r_0 + \varepsilon h(\theta)$ and $h(\theta) = \cos(6\theta)$. Here we take the exponent set $(2, 1, 2, 0)$, $R = 1$, $D = 1$, $r_0 = 0.5$, $\sigma = 10$, and $\varepsilon = 0.01$.

by the radially symmetric solution (3.1) described in Principal Result 3.1. Periodicity in $\theta$ dictates that the angular mode $m$ for the perturbation is an integer on $(-\infty, \infty)$. In our calculation we will allow $m$ to be a positive continuous parameter where we can ignore the complex conjugate without loss of generality.

Since the quasi-steady equilibrium evolves on the slow timescale $T = \epsilon^2 t$, we cannot use a standard linear perturbation expansion in time. Instead we use a WKB ansatz (cf. [3]) of the form

$$v \sim v_e + \Phi\left(\frac{r - r_0}{\epsilon}\right) \mathrm{e}^{im\theta + \varphi(T)/\epsilon^2}, \qquad u \sim u_e + N(r)\mathrm{e}^{im\theta + \varphi(T)/\epsilon^2}, \tag{4.1}$$

where the perturbation in the activator is explicitly made a function of the inner variable only since it will remain localized. Note that, rather than a time dependent amplitude and phase, we place the sole time dependence in the argument of the exponential, as is typical in WKB theory. The interesting impact of the WKB formulation on the stability is the introduction of the integral of the eigenvalue rather than the eigenvalue itself. Owing to the slow time-dependence of the ring solution, delayed transitions to instability, similar to those studied in [39] for the simpler case of 1-D spike solutions, should also occur for ring solutions. Although we will not study such delayed bifurcation effects here for ring solutions, our WKB formulation, which incorporates a historical memory into the linearized system, can in principal be used to analyze this behavior.

We substitute (4.1) into (1.1) taking the GMS forms (1.7) for $g(u, v)$ and $f(u, v)$ and

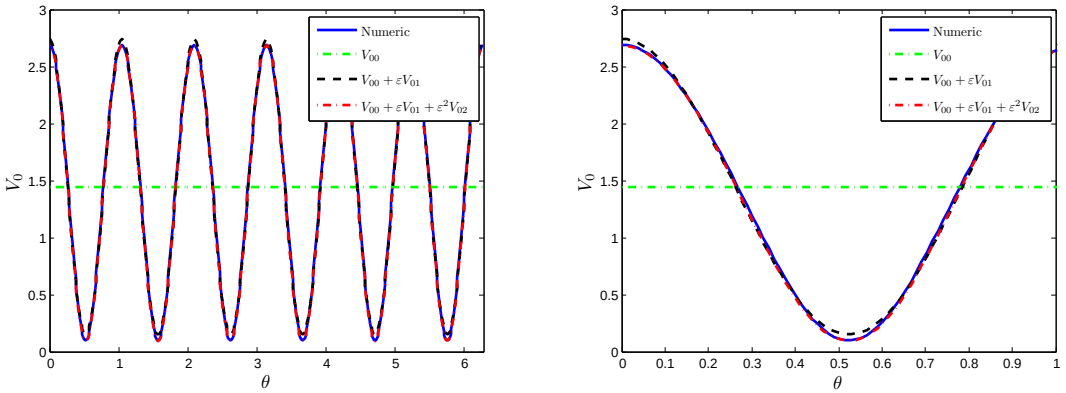


(a) Velocity corrections

(b) Velocity corrections (zoom)

Figure 3.5: Asymptotic corrections compared to full numerical simulations of the curve velocity $V_0$ from solving (2.13) for a perturbed circle with radius $r = r_0 + \varepsilon h(\theta)$ and $h(\theta) = \cos(6\theta)$. Here we take exponent set $(2, 1, 2, 0)$, $R = 1$, $D = 1$, $r_0 = 0.5$, $\sigma = 10$, and $\varepsilon = 0.01$.

linearize the resulting equations. The leading order stability problem for $\Phi$ is

$$L_{0b}\Phi - qU_0^{q-1}\frac{w^2}{(1+bw^2)}N(r_0) = \left(\lambda + \frac{\epsilon^2 m^2}{r_0^2}\right)\Phi\,, \tag{4.2a}$$

$$\text{where} \qquad L_{0b}\Phi \equiv \Phi_{\rho\rho} - \Phi + \frac{2w}{(1+bw^2)^2}\Phi, \qquad \varphi = \int_0^T \lambda(s)\,\mathrm{d}s\,. \tag{4.2b}$$

We note that if $\lambda$ were time-independent then $\varphi/\epsilon^2 = \lambda t$, as expected. Classically, one often takes $\varphi = \lambda t$ regardless of the slow time dependence in the base operator. The WKB method used here more accurately reflects this time dependence but quite often we are only concerned about qualitative eigenvalue information such as regions of positivity and the overall formulation doesn't impact this significantly. Using the Dirac measure, the perturbation to the inhibitor satisfies

$$\frac{1}{r}(rN_r)_r - \frac{m^2}{r^2}N - \theta_\lambda^2 N = \left(\frac{sU_0^{\beta-1}}{D}N(r_0)\mathcal{A} - \frac{oU_0^{\beta-q}}{D}\int_{-\infty}^{\infty} w^{o-1}\Phi\,\mathrm{d}\rho\right)\delta(r-r_0)\,. \tag{4.3}$$

Here $\theta_\lambda = \sqrt{\frac{1+\tau\lambda}{D}}$, where we have chosen the principal branch of the square root. We have the following result concerning the solution to (4.3):

Principal Result 4.1. *The solution to (4.3) subject to $N_r(0) = N_r(R) = 0$ is*

$$N(r) = r_0\left(\frac{oU_0^{\beta-q}}{D}\int_{-\infty}^{\infty} w^{o-1}\Phi\,\mathrm{d}\rho - \frac{sU_0^{\beta-1}}{D}N(r_0)\mathcal{A}\right)\bar{G}_{0,m}(r;r_0)\,, \tag{4.4}$$

*where*

$$\bar{G}_{0,m}(r;r_0) = \begin{cases} \bar{\mathcal{J}}_{m,1}(\theta_\lambda r)\bar{\mathcal{J}}_{m,2}(\theta_\lambda r_0), & 0 \le r \le r_0 \\ \bar{\mathcal{J}}_{m,1}(\theta_\lambda r_0)\bar{\mathcal{J}}_{m,2}(\theta_\lambda r), & r_0 \le r \le R \end{cases}, \tag{4.5a}$$

$$\bar{\mathcal{J}}_{m,1}(\theta_\lambda r) = I_m(\theta_\lambda r), \quad \bar{\mathcal{J}}_{m,2}(\theta_\lambda r) = \bar{\alpha}_m I_m(\theta_\lambda r) + K_m(\theta_\lambda r), \tag{4.5b}$$

$$\bar{\alpha}_m = \left( \frac{K_{m+1}(\theta_\lambda R) - \frac{m}{\theta_\lambda R} K_m(\theta_\lambda R)}{\frac{m}{\theta_\lambda R} I_m(\theta_\lambda R) + I_{m+1}(\theta_\lambda R)} \right). \tag{4.5c}$$

*Furthermore, evaluating (4.4) at $r = r_0$ and using (3.5) to simplify the resulting expression, we get*

$$N(r_0) = U_0^{1-q} \frac{\chi_m}{q} \frac{\int_{-\infty}^{\infty} w^{o-1} \Phi \, \mathrm{d}\rho}{\mathcal{A}}, \qquad \chi_m = \frac{1}{C_m} \equiv qo \left( s + \frac{\mathcal{J}_{0,1}(r_0)\mathcal{J}_{0,2}(r_0)}{\bar{\mathcal{J}}_{m,1}(\theta_\lambda r_0)\bar{\mathcal{J}}_{m,2}(\theta_\lambda r_0)} \right)^{-1}. \tag{4.6}$$

The structure of the eigenvalue problem (4.2a) is such that $\Phi$ has both even and odd solutions. Since $w$ is even, then by (4.6) it follows that $N(r_0)$ can only vanish whenever $\Phi$ is odd, or when $\Phi$ is even with multiple nodal lines. When this happens the eigenvalue, $\lambda$ in (4.2a), becomes part of the spectrum of the local operator $L_{0b}$ in (4.2b). The eigenvalues of this operator are characterized by the following lemma adapted from Theorem 5.4 of [2]:

Lemma 4.1. *Assume that $h(w)$ is such that there is a unique solution to the homoclinic orbit problem*

$$w_{yy} - w + h(w) = 0, \qquad w'(0) = 0, \quad w \to 0 \ \text{ as } \ |y| \to \infty, \quad w(0) > 0,$$

*(for the precise conditions see Lemma 2.1). Then, the corresponding local eigenvalue problem*

$$\mathcal{L}\Phi = \Phi_{yy} - \Phi + h'(w)\Phi = \lambda\Phi, \qquad \Phi \to 0 \quad \text{as} \quad |y| \to \infty,$$

*has a discrete simple positive eigenvalue $\lambda_0 > 0$ associated with a positive eigenfunction $\Phi_0$. There is also a discrete eigenvalue $\lambda_1 = 0$ with the eigenfunction $\Phi_1 = w'$. Furthermore when $h'(0)$ is finite, a continuous spectrum exists on $Re(\lambda) \le -1 + h'(0) < 0$ with $Im(\lambda) = 0$.*

A corollary to Lemma 4.1 is that if other discrete eigenvalues $\lambda_j$, $j > 1$ exist, then $-1 + h'(0) < \lambda_j < 0$. We therefore have two possible cases that lead to instability, i.e. to an eigenvalue with $\mathrm{Re}(\lambda) > 0$. Either $\Phi$ is even and of one sign so that $N(r_0)$ does not vanish, or $\Phi$ is odd (to leading order) and instabilities emerge from $\lambda = 0$. We classify these eigenvalues in a similar manner to [17] whereby the even eigenfunctions that satisfy $\mathrm{Re}(\lambda) > 0$ are called breakup instability modes, and they evolve on an order-one time scale, which is fast relative to the slow dynamics. In contrast, the odd eigenfunctions, that satisfy $\mathrm{Re}(\lambda) \approx 0$, are called zig-zag instability modes, and they evolve on a slow time scale. We will analyze each of these instabilities, recalling that breakup instabilities are the most delicate in terms of studying (2.13).

**4.1. Breakup Instabilities of a Ring.** When $N(r_0) \neq 0$, where $N(r_0)$ is defined in (4.6), then (4.2a) transforms into the following nonlocal eigenvalue problem (NLEP):

Principal Result 4.2. *Let $\epsilon \to 0$ and assume that $\int_{-\infty}^{\infty} w^{o-1}\Phi \,\mathrm{d}\rho \neq 0$. Then, $\Phi$ satisfies the NLEP*

$$L_{0b}\Phi - \frac{\chi_m}{\mathcal{A}}\frac{w^2}{(1+bw^2)}\int_{-\infty}^{\infty} w^{o-1}\Phi \,\mathrm{d}\rho = \mu\Phi\,, \qquad \text{where} \quad \mu \equiv \lambda + \frac{\epsilon^2 m^2}{r_0^2}\,, \tag{4.7}$$

*where we explicitly include terms $\epsilon^2 m^2$ to account for large wavenumber perturbations. Since $L_{0b}$ is self-adjoint, we can alternatively readily show that the unstable eigenvalues are roots in $Re(\lambda) > 0$ of $g_m(\lambda) = 0$, where*

$$g_m(\lambda) \equiv C_m(\lambda) - f(\mu)\,, \qquad f(\mu) \equiv \frac{\int_{-\infty}^{\infty} w^{o-1}\psi \,\mathrm{d}\rho}{\mathcal{A}}\,, \qquad \psi = (L_{0b}-\mu)^{-1}\frac{w^2}{(1+bw^2)}\,. \tag{4.8}$$

*Here $C_m(\lambda)$ is given by (4.6).*

This operator splitting approach is the same technique used to analyze the NLEP for a straight stripe solution in Principal Result 2.2 of [17]. We start with the case $\sigma = b = 0$ where $L_0\Psi = L_{00}\Psi = \nu\Psi$. From [8, 23], the continuous spectrum exists on $\mathrm{Re}(\nu) < -1$ and the discrete eigenvalues and eigenfunctions satisfy,

$$\nu_0 = \frac{5}{4}\,, \quad \Psi_0 = w^{3/2}\,; \quad \nu_1 = 0\,, \quad \Psi_1 = w'\,; \quad \nu_2 = -\frac{3}{4}\,, \quad \Psi_2 = \left(1 - \frac{5}{6}w\right)w^{1/2}\,. \tag{4.9}$$

The analysis of the NLEP (4.7) when $\sigma = 0$ is very similar to that in Appendix A of [17]. Specifically, it relies on the following properties of $f(\mu)$, as rigorously established in Proposition 3.1 and 3.5 of [40]:

$$f'(\mu) > 0\,, \quad \mu \in [0,\nu_0)\,; \qquad f''(\mu) > 0\,, \quad \mu \in [0,\nu_0)\,; \qquad f(\mu) < 0\,, \quad \mu \in (\nu_0,\infty)\,, \tag{4.10}$$

$$f(\mu) \sim 1 + \left(1 - \frac{1}{2o}\right)\mu + \kappa_c\mu^2 \quad \text{as} \quad \mu \to 0\,; \qquad \kappa_c \equiv \frac{\int_{-\infty}^{\infty} w^{o-1}L_0^{-3}(w^2)\,\mathrm{d}\rho}{\mathcal{A}}\,. \tag{4.11}$$

While [40] only demonstrates the properties for $o = 2$ and $o = 3$, they can be extended numerically to general exponents. We also have the following properties for $C_m$ in (4.6), which are readily established through numerical and asymptotic investigation of the modified Bessel functions $I_n$ and $K_n$:

$$C_0(0) = 1/2\,, \qquad \frac{\partial C_m}{\partial m}(0) > 0\,, \qquad \frac{\partial C_m}{\partial \lambda} > 0\,, \qquad \frac{\partial^2 C_m}{\partial \lambda^2} < 0\,, \tag{4.12}$$

as well as $C_m = \mathcal{O}(m)$ for $m \gg 1$.

First we establish the following result regarding the neutral stability points:

Proposition 4.2. *There exists two neutral stability points $m = m_{b^-}$ and $m = m_{b^+}$ that satisfy $g_m(0) = 0$. The lower threshold $m_{b^-}$ satisfies, to leading order, the implicit relation*

$$\mathcal{J}_{m_{b^-},1}(r_0)\mathcal{J}_{m_{b^-},2}(r_0) = \frac{\mathcal{J}_{0,1}(r_0)\mathcal{J}_{0,2}(r_0)}{\beta}\,, \qquad \beta = qo - s\,, \tag{4.13}$$

*while the upper threshold $m_{b^+}$ is given asymptotically for $\epsilon \ll 1$ by*

$$m_{b^+} \sim \frac{r_0\sqrt{\nu_0}}{\epsilon} - \frac{qo\mathcal{B}}{4\nu_0\mathcal{J}_{0,1}(r_0)\mathcal{J}_{0,2}(r_0)}; \qquad \mathcal{B} = \frac{\int_{-\infty}^{\infty} w^2\Psi_0\,\mathrm{d}\rho \int_{-\infty}^{\infty} w^{o-1}\Psi_0\,\mathrm{d}\rho}{\mathcal{A}\int_{-\infty}^{\infty}\Psi_0^2\,\mathrm{d}\rho}. \tag{4.14}$$

*Here $\nu_0$ and $\Psi_0$ are the principal eigenpair of the local operator, as given in (4.9).*

*Proof.* The neutral stability point $m_{b^-}$ is calculated by simply satisfying $g_m(0) = 0$ and using the monotonicity properties (4.12) to ensure its uniqueness. The second neutral stability point, $m_{b^+}$, utilizes an asymptotic expansion in (4.7) of the form $\Phi \sim \epsilon^{-1}\Phi_0 + \Phi_1$ and $m \sim \epsilon^{-1}m_0 + m_1$, to generate the problems

$$L_0\Phi_0 = \frac{m_0^2}{r_0^2}\Phi_0, \qquad L_0\Phi_1 - \frac{m_0^2}{r_0^2}\Phi_1 = \frac{qow^2}{2\mathcal{J}_{0,1}(r_0)\mathcal{J}_{0,2}(r_0)m_0\mathcal{A}}\int_{-\infty}^{\infty} w^{o-1}\Phi_0\,\mathrm{d}\rho + \frac{2m_0m_1}{r_0^2}\Phi_0. \tag{4.15}$$

The first has solution $\Phi_0 = \Psi_0$ and $m^2/r_0^2 = \nu_0$, which becomes a homogeneous solution for the second problem for $\Phi_1$. Invoking a solvability condition generates the required correction term $m_1$. ∎

The eigenvalue analysis now follows identically as in Appendix A of [17]. Specifically, in regards to complex eigenvalues, we can use a winding number criterion (cf. [36]) to count the number of eigenvalues $N$ in the right-half plane $\mathrm{Re}(\lambda) > 0$. This yields

$$N = \frac{5}{4} + \frac{1}{\pi}[\arg g_m]_{\Gamma_I}, \quad 0 < m < \frac{r_0\sqrt{\nu_0}}{\epsilon}; \qquad N = \frac{1}{4} + \frac{1}{\pi}[\arg g_m]_{\Gamma_I}, \quad m > \frac{r_0\sqrt{\nu_0}}{\epsilon}, \tag{4.16}$$

where $\Gamma_I$ is the positive imaginary axis traversed downwards. Overall, we have the following proposition regarding eigenvalues to (4.7) when there is no saturation:

Proposition 4.3. *For $0 \le m < m_{b^-}$, there are no eigenvalues with positive real part when $\tau$ is sufficiently small and two complex eigenvalues with positive real part when $\tau$ is sufficiently large. These eigenvalues undergo a Hopf bifurcation when $\tau = \tau_m^H$. As $\tau$ increases further, the complex conjugate pair coincide on the real axis and become purely real. The neutral stability point at $m = m_{b^-}$ is the largest eigenvalue while $\tau < \tau^*_{m_{b^-}}$ at which point there exists some $\lambda_\tau > 0$ that is purely real. The transition value $\tau = \tau^*_{m_{b^-}}$ occurs at $m = m_{b^-}$ when $g_m(0) = \frac{\mathrm{d}g_m}{\mathrm{d}\lambda}(0) = 0$. For $m_{b^-} < m < m_{b^+}$ there exists exactly one real positive eigenvalue for all $\tau$ and when $m > m_{b^+}$ there are no eigenvalues with positive real part for all $\tau$.*

*Proof.* The proof follows immediately from Appendix A of [17] with the neutral stability points redefined by Proposition 4.2. ∎

A unique aspect of the ring problem that is not present in the stripe case is the curvature term $r_0^{-1}$, which modifies the stability boundaries. This is most readily seen in the expression for $m_{b^+}$, (4.14) where the upper instability boundary grows with increasing circle radius (decreasing curvature). The implication of this qualitative result is that higher curvature circles are less susceptible to high wave mode breakup instabilities than are smaller curvature circles. Table 4.1 shows the values of $m_{b^-}$ and $m_{b^+}$ for various choices of $r_0$ corresponding to the exponent set $(2, 1, 2, 0)$ with $D = 1$, $R = 1$, and $\tau = 0$. We compute $m_{b^+}$ using (4.14) and $m_{b^-}$ by using a Newton's Method solver on (4.13). The lower instability band $m_{b^-}$ also

| $r_0$ | $m_{b^-}$ | $\tau^*_{m_{b^-}}$ | $m_{b^+}$ |
|---|---|---|---|
| 0.01 | 0.1375 | 5.0456 | 0.3629 |
| 0.10 | 0.2266 | 2.9539 | 4.3329 |
| 0.25 | 0.3027 | 2.2126 | 10.9972 |
| 0.50 | 0.4003 | 1.8376 | 22.1376 |
| 0.75 | 0.4920 | 1.8736 | 33.3084 |
| 0.90 | 0.5520 | 2.0969 | 40.0231 |

Table 4.1: Breakup instability boundary limits $m_{b^-}$ and $m_{b^+}$ for various values of $r_0$ subject to the exponent set $(p, q, o, s) = (2, 1, 2, 0)$, $D = 1$, $R = 1$, and $\tau = 0$.

increases with decreasing curvature but to a lesser extent as it remains an $\mathcal{O}(1)$ quantity. Overall, the breakup instability band is suppressed as the curve shrinks. In Table 4.1 we also compute $\tau^*_{m_{b^-}}$, the value of $\tau$ for which the lower instability point vanishes and this decreases with decreasing curvature, which implies that smaller circles maintain the neutral stability point for a larger range of $\tau$. All of this behaviour supports the breakup stabilizing effects that curvature has on the circle. We expect that a similar qualitative result would likely be true for general curves, although the analysis of this is an open problem.

**4.1.1. The Effect of Saturation on the Breakup Instability Band.** When we add saturation, the upper neutral stability point (4.14) of Proposition 4.2 still satisfies $m_{b^+} \sim r_0\sqrt{\nu_0(b)}/\epsilon$ to leading order where $\nu_0(b)$ is the positive discrete eigenvalue to the operator $L_{0b}$ given by (4.2b). Such a unique positive discrete eigenvalue exists because the operator can still be classified by Lemma 4.1, even in the presence of saturation. We start with an important lemma regarding the critical saturation value $b_c$,

Lemma 4.4. *Consider the singular activator limit (2.1) with the saturated GM formulation (2.3). When $0 \leq b < b_c$ with $b_c$ given by (2.6) then a homoclinic orbit exists via Lemma 2.1. When $b = b_c$ a heteroclinic orbit, $\hat{w}$, exists with*

$$\lim_{\hat{\eta}\to-\infty} \hat{w} = 0\,, \qquad \lim_{\hat{\eta}\to\infty} \hat{w} = w_m(b_c)\,, \tag{4.17}$$

*where $w_m(b_c)$ is given by (2.6).*

The proof of this lemma rests on a continued analysis of Lemma 2.1 at the value $b = b_c$ and recognizing that $w_m(b_c)$ is a saddle point in the $w'$ versus $w$ phase-plane. Considering this new heteroclinic orbit, we are lead to the following result:

Principal Result 4.3. *When $b = b_c$ in the saturated GM model, a heteroclinic orbit, $\hat{w}$ exists on $0 < \hat{w} < w_m(b_c)$ by Lemma 4.4 and $\hat{w}'$ is an even function with no nodal lines. As such, by Lemma 4.1, $\hat{w}'$ is the principal eigenfunction of $L_{0b}$ with eigenvalue $\nu_0(b_c) = 0$ and, therefore, the upper neutral stability point $m = m_{b^+}$ tends to zero as $b$ tends to $b_c$.*

When $b = b_c$ then $\hat{w}$ is an equilibrium solution to (2.2). This heteroclinic orbit also has a translational invariance and therefore differentiating (2.2) with respect to the space variables yields $L_{0b}\hat{w}' = 0$ and therefore zero is an eigenvalue of the operator. Since $\hat{w}$ is an even function with no nodal lines then it is the principal eigenvector and hence zero is the principal

eigenvalue. In Fig. 4.1, we numerically verify that the principal eigenvalue $\nu_0(b)$ tends to zero as $b \to b_c^-$. It is an open problem to theoretically predict the explicit rate at which $\nu_0(b)$ tends to zero as $b \to b_c^-$.

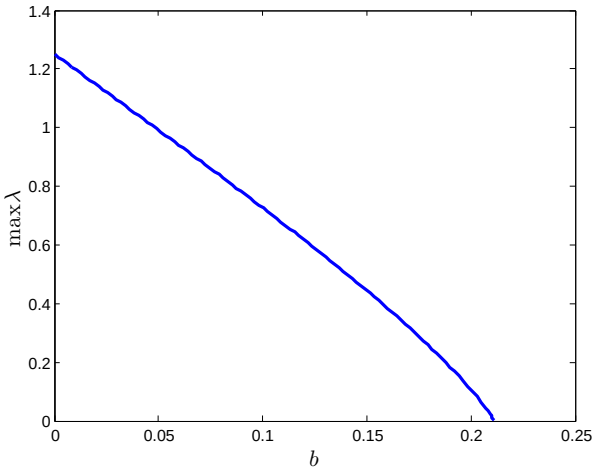


Figure 4.1: Computation of the principal eigenvalue of $L_{0b}$ given by (4.2b) as the saturation $b$ is increased.

The entire classification of the breakup instability regime rested upon having the principal eigenvalue of the NLEP satisfy $\mathrm{Re}(\nu_0) > 0$ so that there was a finite band $m_{b^-} < m < m_{b^+}$ where a real positive eigenvalue existed. However, since this eigenvalue tends to zero at critical saturation, it is reasonable to expect that this can entirely quench the breakup instability behaviour. Indeed, we observe this behaviour numerically in Fig. 4.2 where we plot the principal eigenvalue to the NLEP (4.7) versus $m$ for a range of $b$ values and see that the entire breakup spectrum disappears as we vary saturation. From this plot, we observe that even when $b \approx 0.2 < b_c$ there is no breakup instability band for $m$. It is important to emphasize that Principal Result 4.3 nor Fig. 4.2 should be taken as a proof that the breakup instability can always be suppressed. Indeed for fixed $b$ then as $\epsilon \to 0$ there will always be an $\epsilon^*$ such that for $\epsilon < \epsilon^*$ a breakup instability band will form. However, in our numerical computations we consider $\epsilon$ as a small but fixed parameter and for any fixed $\epsilon$ there will be a range of $b$ values for which $m_{b^+} \ll 1$ suggesting the disappearance of the breakup band. The numerical experiments in §5 support this conjecture.

**4.2. Zig-Zag Instabilities of a Ring.** When $N(r_0) = 0$, the spectrum of (4.2a) reduces to eigenfunctions that belong to $L_{0b}$. Following Lemma 4.1, instability can occur when $\Phi \sim w_\rho$ and $\mu = \lambda + \epsilon^2 m^2 / r_0^2 \sim 0$ to leading order. We first remark that if $m = \mathcal{O}(\epsilon^{-1})$ then $\mu = 0$ implies $\mathrm{Re}(\lambda) < 0$ and so instability can only occur where $m = \mathcal{O}(1)$. Secondly, unlike the study of breakup instabilities, which followed from an analysis similar to [17], the analysis here for zig-zag instabilities is both novel and intricate owing to the radial geometry. In particular, Appendix B of [17] for the zigzag instabilities associated with a straight, planar, stripe solution

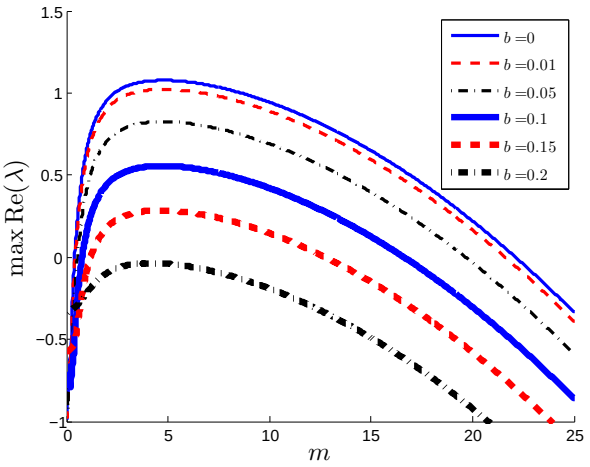


Figure 4.2: Computation of eigenvalues of the NLEP for $b > 0$ and $\tau = 0$ as the mode $m$ is varied. In all cases $(2, q, o, s) = (2, 1, 2, 0)$, $\epsilon = 0.025$, $R = 1$, $r_0 = 0.5$, and $D = 1$.

relies on commutation of the $L_0$ operator with differentiation, which does not extend to our problem with radial geometry due to the presence of the curvature $r^{-1}$ term. We therefore must use a rather intricate matched asymptotic analysis to analyze zigzag instabilities of a ring. This method could also be applied to the stripe case in [17] and as such is a more general approach to the analysis of zig-zag instabilities.

Since $N(r_0) \sim 0$ to leading order, we rescale $N(r) = \epsilon\hat{N}$, and let $\tilde{N}(\rho) = \hat{N}(r_0 + \epsilon\rho)$. We then introduce the following expansion into the spectral problem:

$$\Phi \sim w_\rho + \epsilon\Phi_1 + \epsilon^2\Phi_2 + \dots\,, \quad \tilde{N}(\rho) \sim \tilde{N}_0 + \epsilon\tilde{N}_1 + \dots\,. \tag{4.18}$$

This leads to our next result regarding eigenvalues at $\mathcal{O}(\epsilon)$:

Proposition 4.5. *Consider $N(r) = \epsilon\hat{N}$ so that $N(r_0) = 0$ to leading order in (4.2a). Expand $\Phi$ and $\tilde{N}(\rho) = \hat{N}(r_0 + \epsilon\rho)$ as in (4.18). Then $\lambda = o(\epsilon)$.*

*Proof.* Let $\lambda = \epsilon\lambda_1$. We start by expanding the equilibrium states as

$$\tilde{v}_e \sim U_0^q w + \epsilon\tilde{v}_1 + \epsilon^2\tilde{v}_2 + \dots\,, \quad \tilde{u}_e \sim U_0 + \epsilon\tilde{u}_1 + \epsilon^2\tilde{u}_2 + \dots\,. \tag{4.19}$$

Upon using (2.7) for the GMS kinetics (1.7), and converting to polar coordinates, we obtain that $\tilde{v}_1$ and $\tilde{u}_1$ satisfy

$$L_{0b}\tilde{v}_1 = -\frac{U_0^q}{r_0}w_\rho + qU_0^{q-1}\frac{w^2}{(1+bw^2)}\tilde{u}_1 - U_0^q\frac{\mathrm{d}r_0}{\mathrm{d}T}w_\rho\,, \tag{4.20a}$$

$$\tilde{u}_{1\rho\rho} = -\frac{1}{D}U_0^\beta w^o\,. \tag{4.20b}$$

If we differentiate (4.20a) with respect to $\rho$ and rearrange the resulting expression we get

$$a_1 w_\rho = -\frac{1}{U_0^q}L_{0b}\tilde{v}_{1\rho} - \frac{w_{\rho\rho}}{r_0} + \frac{q}{U_0}\frac{w^2}{(1+bw^2)}\tilde{u}_{1\rho} - \frac{\mathrm{d}r_0}{\mathrm{d}T}w_{\rho\rho}\,, \tag{4.21}$$

where we have defined $a_1$ by

$$a_1 \equiv \frac{2}{U_0(1+bw^2)^2}\left(\frac{(1-3bw^2)}{U_0^{q-1}(1+bw^2)}\tilde{v}_1 - qw\tilde{u}_1\right). \tag{4.22}$$

In this derivation we used the simplification

$$(L_{0b}y)_\rho = L_{0b}y_\rho + 2\frac{(1-3bw^2)}{(1+bw^2)^3}w_\rho y\,. \tag{4.23}$$

We now proceed with the eigenvalue calculation by substituting the expansion (4.18) into (4.2a) to obtain that $\Phi_1$ satisfies

$$L_{0b}\Phi_1 = -\frac{w_{\rho\rho}}{r_0} - w_{\rho\rho}\frac{\mathrm{d}r_0}{\mathrm{d}T} - a_1 w_\rho + \frac{qU_0^{q-1}}{1+bw^2}w^2\tilde{N}_0 + \lambda_1 w\,, \tag{4.24}$$

which, after using (4.21), reduces to

$$L_{0b}\Phi_1 = \frac{1}{U_0^q}L_{0b}\tilde{v}_{1\rho} + \frac{q}{U_0}\frac{w^2}{(1+bw^2)}\tilde{\mathcal{F}}_0 + \lambda_1 w_\rho\,, \qquad \tilde{\mathcal{F}}_0 = U_0^q\tilde{N}_0 - \tilde{u}_1'\,. \tag{4.25}$$

By Lemma 4.1, $w_\rho$ is a homogeneous solution to this problem, which then leads to the solvability condition

$$\frac{q}{U_0}\int_{-\infty}^{\infty}\frac{w^2}{(1+bw^2)}\tilde{\mathcal{F}}_0 w_\rho\,\mathrm{d}\rho + \lambda_1\int_{-\infty}^{\infty}w_\rho^2\,\mathrm{d}\rho = 0\,, \tag{4.26}$$

where we have used the fact that $L_{0b}$ is a self-adjoint operator in order to remove the first term. To show that the first integral in (4.26) vanishes, we need to study the problem $\tilde{\mathcal{F}}_{0\rho} = U_0^q\tilde{N}_{0\rho} - \tilde{u}_{1\rho\rho}$ which we have differentiated from (4.25) since it is natural to use (4.20b) for $\tilde{u}_{1\rho\rho}$. For $\tilde{N}$, we consider the linearization of (1.1) via (4.1) in the inner region, i.e. we take (4.3) without the using the Dirac measure reduction. This yields,

$$\epsilon^3\tau\tilde{N}\lambda_1 = \frac{D}{(r_0+\epsilon\rho)}((r_0+\epsilon\rho)\tilde{N}_\rho)_\rho - \epsilon^2\frac{Dm^2}{(r_0+\epsilon\rho)^2}\tilde{N} - \epsilon^2\tilde{N} + \frac{o\tilde{v}_e^{o-1}}{{\tilde{u}_e}^s}\Phi - \epsilon\frac{s\tilde{v}_e^o}{\tilde{u}_e^{s+1}}\tilde{N}\,, \tag{4.27}$$

and therefore, using the expansion (4.18), we get $\tilde{N}_{0\rho\rho} = -\frac{oU_0^{\beta-q}}{D}w^{o-1}w_\rho$. Combining this relation with (4.20b) yields $\tilde{\mathcal{F}}_{0\rho} = 0$, which shows that $\tilde{\mathcal{F}}_0$ is constant. Because $\tilde{\mathcal{F}}_0$ is constant, the first integral in (4.26) is odd and, consequently, vanishes. Therefore, $\lambda_1 = 0$ and $\lambda \ll \mathcal{O}(\epsilon)$ as stated. ■

We now use the same techniques at $\mathcal{O}(\epsilon^2)$ to show that eigenvalues are non-vanishing at this order. To do this we will require some key results. Firstly, we have the following result regarding the equilibrium solution at $\mathcal{O}(\epsilon^2)$:

Principal Result 4.4. *Consider $v_e$ and $u_e$ which satisfy (1.5) subject to GMS functions (1.7). If we pose an expansion as (4.19) then $v_1$ and $u_1$ are given by (4.20), while $v_2$ and $u_2$ satisfy,*

$$L_{0b}\tilde{v}_2 = -\frac{\tilde{v}_{1\rho}}{r_{00}} + \frac{\rho U_0^q}{r_{00}^2}w_\rho - \frac{\mathrm{d}r_{00}}{\mathrm{d}T}\tilde{v}_{1\rho} - \frac{\mathrm{d}r_{01}}{\mathrm{d}T}U_0^q w_\rho - \frac{U_0^{q-2}q(q+1)}{2}\frac{w^2}{(1+bw^2)}\tilde{u}_1^2\,,$$
$$+\frac{2q}{U_0}\frac{w}{(1+bw^2)^2}\tilde{u}_1\tilde{v}_1 - \frac{1}{U_0^q}\frac{(1-3bw^2)}{(1+bw^2)^3}\tilde{v}_1^2 + U_0^{q-1}q\frac{w^2}{(1+bw^2)}\tilde{u}_2, \tag{4.28a}$$
$$\tilde{u}_{2\rho\rho} = \frac{U_0}{D} - \frac{\tilde{u}_{1\rho}}{r_{00}} + \frac{1}{D}U_0^{\beta-1}sw^o\tilde{u}_1 - \frac{1}{D}U_0^{\beta-q}ow^{o-1}\tilde{v}_1\,, \tag{4.28b}$$

*where $r_0 = r_{00} + \epsilon r_{01}$. Here, $r_{00}$ replaces $r_0$, i.e. it satisfies (3.7), while $r_{01}$ will satisfy a differential equation via an orthogonality condition with the homogeneous solution $\tilde{v}_2 = w_\rho$ which exists by Lemma 4.1. Differentiating (4.28a) and rearranging yields,*

$$a_2 w_\rho = -\frac{1}{U_0^q}L_{0b}\tilde{v}_{2\rho} - \frac{\tilde{v}_{1\rho\rho}}{U_0^q r_{00}} + \frac{w_\rho}{r_{00}^2} + \frac{\rho w_{\rho\rho}}{r_{00}^2} - \frac{1}{U_0^q}\frac{\mathrm{d}r_{00}}{\mathrm{d}T}\tilde{v}_{1\rho\rho}$$
$$-\frac{\mathrm{d}r_{01}}{\mathrm{d}T}w_{\rho\rho} + \bar{a}_2\tilde{u}_{1\rho} - \frac{a_1}{U_0^q}\tilde{v}_{1\rho} + \frac{q}{U_0}\frac{w^2}{(1+bw^2)}\tilde{u}_{2\rho}\,, \tag{4.29}$$

*where $a_2$ and $\bar{a}_2$ are defined by*

$$a_2 \equiv \frac{2}{U_0(1+bw^2)^2}\left(\frac{(1-3bw^2)}{U_0^{q-1}(1+bw^2)}\tilde{v}_2 - qw\tilde{u}_2\right) + \frac{q(q+1)}{U_0^2}\frac{w}{(1+bw^2)^2}\tilde{u}_1^2$$
$$-\frac{2q}{U_0^{q+1}}\frac{(1-3bw^2)}{(1+bw^2)^3}\tilde{u}_1\tilde{v}_1 - \frac{12bw}{U_0^{2q}}\frac{(1-bw^2)}{(1+bw^2)^4}\tilde{v}_1^2\,, \tag{4.30a}$$
$$\bar{a}_2 \equiv \frac{2q}{U_0^{q+1}}\frac{w}{(1+bw^2)^2}\tilde{v}_1 - \frac{q(q+1)}{U_0^2}\frac{w^2}{(1+bw^2)}\tilde{u}_1\,. \tag{4.30b}$$

It may seem erroneous to introduce a radial correction $r_{01}$ without any consideration to matching conditions in earlier discussions. However, in terms of the outer problem, we are only interested in the singular limit solution where all variables are $\mathcal{O}(1)$ and matching terms generated by radial corrections furnish conditions on terms smaller than $\mathcal{O}(1)$. Next, we establish the following result regarding the eigenfunction solution $\Phi_1$:

Principal Result 4.5. *Consider $\Phi_1$, the eigenfunction correction at $\mathcal{O}(\epsilon)$, which satisfies (4.25) with $\lambda_1 = 0$, as shown in Proposition 4.5. We rewrite this problem as*

$$L_{0b}\left(\Phi_1 - \frac{1}{U_0^q}\tilde{v}_{1\rho} - \frac{q\tilde{\mathcal{F}}_0}{U_0}\psi\right) = 0\,, \qquad L_{0b}\psi = \frac{w^2}{1+bw^2}\,, \tag{4.31}$$

*which, by setting the homogeneous solution to zero without loss of generality, can be solved to yield*

$$\Phi_1 = \frac{1}{U_0^q}\tilde{v}_{1\rho} + \frac{q\tilde{\mathcal{F}}_0}{U_0}\psi\,. \tag{4.32}$$

*In [40], where $b = 0$, it was shown that $\psi = w$. If we operate $L_{0b}$ on this function when $b \neq 0$ then*

$$L_{0b} w = \frac{w^2}{1 + bw^2} \left( \frac{1 - bw^2}{1 + bw^2} \right) . \tag{4.33}$$

*Furthermore, if we recall the homoclinic orbit problem (2.2) and differentiate with respect to the saturation parameter $b$ then we get the result*

$$L_{0b} w_b = \frac{w^4}{(1 + bw^2)^2} . \tag{4.34}$$

*Combining this with (4.33), we have that*

$$L_{0b} w + 2b L_{0b} w_b = \frac{w^2}{1 + bw^2} , \tag{4.35}$$

*and therefore,*

$$\psi = w + 2b w_b , \tag{4.36}$$

*where we have, once again, set the homogeneous solution to zero without loss of generality.*

Using Principal Results 4.4 and 4.5 while taking $\lambda = \epsilon^2 \lambda_2$, we have the following problem for the eigenfunction correction at $\mathcal{O}(\epsilon^2)$:

$$\begin{aligned} L_{0b} \Phi_2 =& \frac{q}{U_0} \frac{w^2}{(1 + bw^2)} \tilde{\mathcal{F}}_1 + \left( \bar{a}_2 - \frac{q}{U_0} \left( a_1 \psi + \frac{1}{r_{00}} \psi_\rho + \frac{\mathrm{d} r_{00}}{\mathrm{d} T} \psi_\rho \right) \right) \tilde{\mathcal{F}}_0 \\ &+ \frac{1}{U_0^q} L_{0b} \tilde{v}_{2\rho} + \left( \lambda_2 + \frac{m^2 - 1}{r_{00}^2} \right) w_\rho , \end{aligned} \tag{4.37a}$$

$$\tilde{\mathcal{F}}_1 = U_0^q \tilde{N}_1 - \tilde{u}_{2\rho} . \tag{4.37b}$$

Since $\Phi_2 = w_\rho$ is a homogeneous solution then the eigenvalue $\lambda_2$ will be be determined by the orthogonality condition

$$\begin{aligned} &\frac{q}{U_0} \underbrace{\int_{-\infty}^{\infty} \frac{w^2}{(1 + bw^2)} w_\rho \tilde{\mathcal{F}}_1 \, \mathrm{d}\rho}_{I_1} + \tilde{\mathcal{F}}_0 \underbrace{\int_{-\infty}^{\infty} \bar{a}_2 w_\rho - \frac{q}{U_0} \left( a_1 \psi w_\rho + \frac{1}{r_{00}} \psi_\rho w_\rho + \frac{\mathrm{d} r_{00}}{\mathrm{d} T} \psi_\rho w_\rho \right) \mathrm{d}\rho}_{I_2} \\ &+ \left( \lambda_2 + \frac{m^2 - 1}{r_{00}^2} \right) \int_{-\infty}^{\infty} w_\rho^2 \, \mathrm{d}\rho = 0 . \end{aligned} \tag{4.38}$$

We will evaluate each of these integrals separately. Beginning with $I_2$, we use (4.21) and integrate by parts to obtain that

$$\int_{-\infty}^{\infty} a_1 \psi w_\rho \, \mathrm{d}\rho = \int_{-\infty}^{\infty} -\frac{1}{U_0^q} \psi L_{0b} \tilde{v}_{1\rho} + \frac{w_\rho \psi_\rho}{r_{00}} + \frac{q}{U_0} \psi \tilde{u}_{1\rho} \frac{w^2}{(1 + bw^2)} + \frac{\mathrm{d} r_{00}}{\mathrm{d} T} w_\rho \psi_\rho \, \mathrm{d}\rho . \tag{4.39}$$

Using (4.30b) from Principal Result 4.4, integrating by parts, and using the self-adjoint property of $L_{0b}$, we also have that

$$\int_{-\infty}^{\infty} \bar{a}_2 w_\rho \,\mathrm{d}\rho = -\frac{q}{U_0^{q+1}} \int_{-\infty}^{\infty} \psi L_{0b} \tilde{v}_{1\rho} \,\mathrm{d}\rho + \frac{q(q+1)}{2U_0^2} \hat{\mathcal{H}} \left\langle \frac{\mathrm{d}u_e}{\mathrm{d}r} \right\rangle_{r_{00}} \int_{-\infty}^{\infty} w_\rho^2 \,\mathrm{d}\rho \,. \tag{4.40}$$

Here $\hat{\mathcal{H}}$ is given in (3.7), while $\langle \frac{\mathrm{d}u_e}{\mathrm{d}r} \rangle_{r_{00}}$ denotes the average value of the outer inhibitor derivative solution across $r = r_{00}$. Upon combining these two integrals we get

$$\begin{aligned} I_2 = \frac{q(q+1)}{2U_0^2} \hat{\mathcal{H}} \left\langle \frac{\mathrm{d}u_e}{\mathrm{d}r} \right\rangle_{r_{00}} \int_{-\infty}^{\infty} w_\rho^2 \,\mathrm{d}\rho - \frac{q^2}{U_0^2} \int_{-\infty}^{\infty} \psi \tilde{u}_{1\rho} \frac{w^2}{(1+bw^2)} \,\mathrm{d}\rho \\ - \frac{2q}{U_0} \left( \frac{1}{r_{00}} + \frac{\mathrm{d}r_{00}}{\mathrm{d}T} \right) \int_{-\infty}^{\infty} w_\rho \psi_\rho \,\mathrm{d}\rho \,. \end{aligned} \tag{4.41}$$

For the last integral, we simplify it using (3.7), to finally obtain, after integrating several terms by parts and by using (4.36) for $\psi$, that

$$\begin{aligned} I_2 = &\frac{q}{2U_0^2} \hat{\mathcal{H}} \left\langle \frac{\mathrm{d}u_e}{\mathrm{d}r} \right\rangle_{r_{00}} \int_{-\infty}^{\infty} w_\rho^2 \,\mathrm{d}\rho - \frac{bq^2}{U_0^2} \left\langle \frac{\mathrm{d}u_e}{\mathrm{d}r} \right\rangle_{r_{00}} \left( 4 \int_0^{\infty} \frac{w^2 w_b}{(1+bw^2)} \,\mathrm{d}\rho \right. \\ &\left. + 4 \int_0^{\infty} \int_0^{w} \frac{v^4}{(1+bv^2)^2} \,\mathrm{d}v \,\mathrm{d}\rho - 2\hat{\mathcal{H}} \int_{-\infty}^{\infty} w_\rho w_{b\rho} \,\mathrm{d}\rho \right) . \end{aligned} \tag{4.42}$$

We make one further simplification by differentiating $\hat{\mathcal{H}}$ in (3.7) with respect to the saturation $b$, and noticing that this is the final term in the brackets in (4.42). Therefore, we arrive at

$$I_2 = \frac{q}{2U_0^2} \hat{\mathcal{H}} \left\langle \frac{\mathrm{d}u_e}{\mathrm{d}r} \right\rangle_{r_{00}} \int_{-\infty}^{\infty} w_\rho^2 \,\mathrm{d}\rho \left( 1 - \frac{2bq}{\hat{\mathcal{H}}} \frac{\mathrm{d}\hat{\mathcal{H}}}{\mathrm{d}b} \right) . \tag{4.43}$$

Finally, we consider $I_1$ in (4.38) which, upon integrating by parts, is

$$I_1 = -\frac{\hat{\mathcal{H}}}{4} \int_{-\infty}^{\infty} w_\rho^2 \,\mathrm{d}\rho \left( \tilde{\mathcal{F}}_{1\rho}(\infty) + \tilde{\mathcal{F}}_{1\rho}(-\infty) \right) + \int_{-\infty}^{\infty} \left( \int_0^{\rho} \int_0^{w(x)} \frac{v^2}{1+bv^2} \,\mathrm{d}v \,\mathrm{d}x \right) \tilde{\mathcal{F}}_{1\rho\rho} \,\mathrm{d}\rho \,, \tag{4.44}$$

where the term in brackets of the second integral is an odd function of $\rho$. To see that this integral vanishes, we require the following result regarding $\tilde{\mathcal{F}}_1$:

Principal Result 4.6. *Consider $\tilde{\mathcal{F}}_1$ defined by (4.37b), and differentiate it twice with respect to $\rho$ to get*

$$\tilde{\mathcal{F}}_{1\rho\rho} = U_0^q \tilde{N}_{\rho\rho} - \tilde{u}_{2\rho\rho\rho} \,. \tag{4.45}$$

*The third derivative of $u_2$ is obtained by differentiating (4.28b) in Principal Result 4.4. We obtain an equation for $\tilde{N}_1$ from an expansion to $\mathcal{O}(\epsilon)$ of (4.27) using (4.18) to produce,*

$$\begin{aligned} \tilde{N}_{1\rho\rho} = &- \frac{\tilde{N}_{0\rho}}{r_{00}} + \frac{sU_0^{\beta-1}}{D} w^o \tilde{N}_0 - \frac{oU_0^{\beta-q}}{D} w^{o-1} \left( \frac{\tilde{v}_{1\rho}}{U_0^q} + \frac{q\tilde{\mathcal{F}}_0}{U_0} \psi \right) \\ &+ \frac{osU_0^{\beta-q-1}}{D} w^{o-1} w_\rho \tilde{u}_1 - \frac{o(o-1)U_0^{\beta-2q}}{D} w^{o-2} w_\rho \tilde{v}_1 \,. \end{aligned} \tag{4.46}$$

*Combining this with the third derivative of $\tilde{u}_2$ yields*

$$\tilde{\mathcal{F}}_{1\rho\rho} = \frac{U_0^{\beta-1}}{D} w^{o-1} \tilde{\mathcal{F}}_0(sw - o\psi)\,, \tag{4.47}$$

*which is an even function. Therefore, in (4.44),*

$$\int_{-\infty}^{\infty} \left( \int_0^{\rho} \int_0^{w(x)} \frac{v^2}{1+bv^2}\,\mathrm{d}v\,\mathrm{d}x \right) \tilde{\mathcal{F}}_{1\rho\rho}\,\mathrm{d}\rho = 0\,. \tag{4.48}$$

If we define a global function $\mathcal{F} = U_0^q \hat{N} - \frac{\mathrm{d}u_e}{\mathrm{d}r}$ and combine $I_2$ and $I_1$, we have that (4.38) simplifies to

$$\lambda_2 = \frac{1-m^2}{r_{00}^2} - \frac{q}{2U_0^2}\hat{\mathcal{H}}\left(1 - \frac{2bq}{\hat{\mathcal{H}}}\frac{\mathrm{d}\hat{\mathcal{H}}}{\mathrm{d}b}\right)\left\langle \frac{\mathrm{d}u_e}{\mathrm{d}r}\right\rangle_{r_{00}} \mathcal{F}(r_{00}) + \frac{q\hat{\mathcal{H}}}{2U_0}\left(U_0^q \left\langle \frac{\mathrm{d}\hat{N}}{\mathrm{d}r}\right\rangle_{r_{00}} - \left\langle \frac{\mathrm{d}^2 u_e}{\mathrm{d}r^2}\right\rangle_{r_{00}}\right), \tag{4.49a}$$

$$\mathcal{F}(r_{00}) = U_0^q \left\langle \hat{N}\right\rangle_{r_{00}} - \left\langle \frac{\mathrm{d}u_e}{\mathrm{d}r}\right\rangle_{r_{00}}, \tag{4.49b}$$

i.e. the eigenvalues can be written in terms of outer solutions to $u_e$ and $\hat{N}$. Here we have used the fact that $\tilde{\mathcal{F}}$ is a constant to leading order and therefore that $\mathcal{F}(r_{00})$ must be defined and equal to the average value. Next, we establish the following result regarding the outer inhibitor eigenfunction $\hat{N}$:

Principal Result 4.7. *Approximating the localized radius $r_0 = r_{00} + \epsilon r_{01} \approx r_{00}$, the problem for the inhibitor eigenfunction in the outer region takes the form*

$$\frac{1}{r}(r\hat{N}_r)_r - \frac{m^2}{r^2}\hat{N} - \frac{1}{D}\hat{N} + \underbrace{\frac{1}{\epsilon^2}\frac{o}{D}\frac{v_e^{o-1}}{u_e^s}\Phi\left(\frac{r-r_{00}}{\epsilon}\right) - \frac{1}{\epsilon}\frac{s}{D}\frac{v_e^o}{u_e^{s+1}}\hat{N}}_{S_1} = 0\,. \tag{4.50}$$

*Taking $\epsilon \to 0$, the terms $S_1$ lead to singularities with Dirac measures of the form*

$$S_1 = \frac{U_0^{\beta-q}}{D}\mathcal{A}\,\delta'(r-r_{00}) + \frac{U_0^{\beta-q-1}}{D}\mathcal{F}(r_{00})\mathcal{A}\left(\beta + \frac{2qb}{\mathcal{A}}\frac{\mathrm{d}\mathcal{A}}{\mathrm{d}b}\right)\delta(r-r_{00})\,, \tag{4.51}$$

*with $\mathcal{A}$, $U_0$, and $\beta$ given by (3.5), and $\mathcal{F}(r_{00})$ by (4.49b). Here $\delta'(\cdot)$ is the Dirac measure of order one. Substituting these singularities into (4.50) and integrating yields the jump relations*

$$[\hat{N}]_{r_{00}} = -\frac{\bar{A}_0}{U_0^q}\,, \tag{4.52a}$$

$$\left[\frac{\mathrm{d}\hat{N}}{\mathrm{d}r}\right]_{r_{00}} = \frac{\bar{A}_0}{U_0^q r_{00}} - \frac{\bar{A}_0\bar{\bar{A}}_0}{U_0^{q+1}}U_0^q\left\langle \hat{N}\right\rangle_{r_{00}} + \frac{\bar{A}_0\bar{\bar{A}}_0}{U_0^{q+1}}\left\langle \frac{\mathrm{d}u_e}{\mathrm{d}r}\right\rangle_{r_{00}}, \tag{4.52b}$$

*where* $\bar{A}_0$ *and* $\bar{\bar{A}}_0$ *are defined by (3.15). If we define*

$$\mathcal{Z} \equiv H_n U_0^q \hat{N} + \mathcal{V}_{1n}\,, \qquad H_n \equiv \frac{1}{2\pi}\int_0^{2\pi} h(\theta)\exp(-in\theta)\,\mathrm{d}\theta\,, \tag{4.53}$$

*where* $h(\theta)$ *is a smooth* $C^2$ *periodic function and* $\mathcal{V}_{1n}$ *is the solution in Principal Result 3.2, it follows that the outer inhibitor eigenfunction problem can be recast as*

$$\frac{1}{r}(r\mathcal{Z}_r)_r - \frac{n^2}{r^2}\mathcal{Z} - \frac{1}{D}\mathcal{Z} = 0\,, \qquad r \neq r_{00}\,; \qquad \left.\frac{\mathrm{d}\mathcal{Z}}{\mathrm{d}r}\right|_{r=r_{00}} = 0\,, \tag{4.54a}$$

$$[\mathcal{Z}]_{r_{00}} = 0\,, \qquad \left[\frac{\mathrm{d}\mathcal{Z}}{\mathrm{d}r}\right]_{r_{00}} = -\frac{\bar{A}_0\bar{\bar{A}}_0}{U_0}\mathcal{Z}(r_{00})\,, \tag{4.54b}$$

*for which* $\mathcal{Z} \equiv 0$ *is the only solution. Therefore, the outer inhibitor eigenfunction is simply*

$$\hat{N} = -\frac{1}{H_n U_0^q}\mathcal{V}_{1n}\,. \tag{4.55}$$

The Dirac measure singular terms in Principal Result 4.7 arise in a similar fashion to (2.12) after expanding $\Phi$ and $\hat{N} = \tilde{N}((r-r_0)/\epsilon)$ using (4.18) while the order one Dirac measure term comes from recognizing that,

$$\lim_{\epsilon\to 0}\frac{w^o\left(\frac{r-r_0}{\epsilon}\right)}{\epsilon} = \mathcal{A}\delta(r-r_0)\,, \tag{4.56}$$

and then differentiating the result. Overall, we are lead to the final key result for the small eigenvalues associated with the zig-zag mode, and which demonstrates the close connection between these eigenvalues and the quasi-steady near-circle problem already discussed:

Principal Result 4.8. *Consider a radially symmetric quasi-steady state given by (3.1) in Principal Result 3.1 with dynamic condition subject to (3.7). Assume that these steady-states are perturbed in the sense of (4.1) with* $\Phi$ *odd so that* $N(r) = \epsilon\hat{N}$ *with* $\hat{N}$ *given by (4.55) in Principal Result 4.7. The leading order time expansion satisfies* $\varphi(T)/\epsilon^2 = \int_0^T \lambda_m(s)\,\mathrm{d}s$ *with*

$$\begin{aligned}\lambda_m =& \frac{1-m^2}{r_{00}^2} + \frac{q}{2H_m U_0^2}\hat{\mathcal{H}}\left(1 - \frac{2bq}{\hat{\mathcal{H}}}\frac{\mathrm{d}\hat{\mathcal{H}}}{\mathrm{d}b}\right)\left\langle\frac{\mathrm{d}u_e}{\mathrm{d}r}\right\rangle_{r_{00}}\left(\langle\mathcal{V}_{1m}\rangle_{r_{00}} + H_m\left\langle\frac{\mathrm{d}u_e}{\mathrm{d}r}\right\rangle_{r_{00}}\right)\\ &- \frac{q\hat{\mathcal{H}}}{2H_m U_0}\left(\left\langle\frac{\mathrm{d}\mathcal{V}_{1m}}{\mathrm{d}r}\right\rangle_{r_{00}} + H_m\left\langle\frac{\mathrm{d}^2u_e}{\mathrm{d}r^2}\right\rangle_{r_{00}}\right)\,.\end{aligned} \tag{4.57}$$

*In terms of the near circular ring geometry* $r = r_0 + \varepsilon h(\theta)$, $\varepsilon \ll 1$ *which has leading order correction given by Principal Result 3.2, the leading order velocity correction satisfies*

$$V_{01} = \sum_{m=-\infty}^{\infty} H_m\lambda_m\exp(im\theta)\,. \tag{4.58}$$

We can see the eigenvalue-velocity relationship more naturally by looking at the activator itself. If the eigenfunction is odd then the the maximum of $\Phi$ is not at $\rho = 0$. This maximal location $\rho^*$ is how we define the localization curve for the activator $v$. Therefore, extending back into the outer coordinates, the localization curve will be at the radius $r = r_0 + \epsilon\rho^*(\theta)$ where

$$\tilde{v}_\rho(\rho^*) = \tilde{v}_{e\rho}(\rho^*) + \Phi_\rho(\rho^*) \exp\left( im\theta + \int_0^T \lambda_m(s)\,\mathrm{d}s \right) = 0\,. \tag{4.59}$$

Since this maximal radius is a function of the angle, we produce the aforementioned zig-zag instability which creates a near circle perturbation. If we differentiate (4.59) with respect to $T$ then we can write the curve velocity as

$$\frac{\mathrm{d}r}{\mathrm{d}T} = \frac{\mathrm{d}r_0}{\mathrm{d}T} + \epsilon\frac{\mathrm{d}\rho^*}{\mathrm{d}T} = \frac{\mathrm{d}r_0}{\mathrm{d}T} + \epsilon\frac{\tilde{v}_{e\rho}(\rho^*)}{\tilde{v}_{\rho\rho}(\rho^*)}\lambda_m(T)\,, \tag{4.60}$$

with $\frac{\mathrm{d}r_0}{\mathrm{d}T}$ given by (3.7). This explicitly shows the velocity-eigenvalue relationship when the coefficient in front of $\lambda_m$ is small.

## 5. Numerical Experiments in the Semi-Strong Regime.

We now compute full numerical solutions to (1.1) for the GMS nonlinearities (1.7) for the exponent set $(2, 1, 2, 0)$. From an analysis perspective, it is often convenient to scale the diffusivity to be unity and alter the length scale. However, this is generally impractical when computing. Instead, we fix $R = 1$ and instead vary the diffusion coefficient. As we remarked in §3, these two formulations are not invariant when saturation is included in that different values of $\sigma$ are needed to generate a given value of $b$. In our simulations, we fix $b$ initially and adjust $\sigma$ accordingly for a given parameter regime. For the discretization, we take a uniformly spaced rectangular grid in $(r, \theta)$ with a cell centered discretization. We supplement this with Neumann conditions at $r = 1$ and a compatibility condition that the derivative of each component vanish at $r = 0$. For plotting purposes, we use a conformal map to a circle using Matlab's `pol2cart` function.

To stimulate breakup instabilities, we will allow for random perturbations to the base state when $b = 0$, which is sampled uniformly from $[-\delta, \delta]$ with $\delta = 0.001$. Even when we allow saturation to be non-zero, we take the $b = 0$ base solution and allow the code to evolve naturally to a quasi-equilibrium. When breakup patterns do occur, we expect that the maximal eigenvalue will persist but as we discussed in Proposition 4.3, there is usually a range of instability and, due to the random perturbations, modes clustered near the maximal mode may persist. Therefore, when looking for breakup patterns, we perform a discrete Fourier transform of the solution and isolate the modes that are within 95% of the maximal mode (herein termed *dominant modes*). Since we are not concerned with translational effects, we will filter the $m = 0$ mode. Since $m$ are integers then we predict the number of spots, $N$, that form to be $N = m_{\mathrm{dom}}$. When breakup patterns are not expected, we will instead consider a perturbation of the form $r = r_0 + 0.02\cos(6\theta)$. Since slow dynamics occur on the long time scale $\mathcal{O}(\epsilon^{-2})$, we will track the curve base radius $r_0$ as the average $r$ position which produces the largest value of the activator, $v$, for each $\theta$. If the ring breaks into spots, this value is not reliable or relevant, and secondary instabilities intrinsic to spot patterns (cf. [19] for the Schnakenburg model) can take effect.

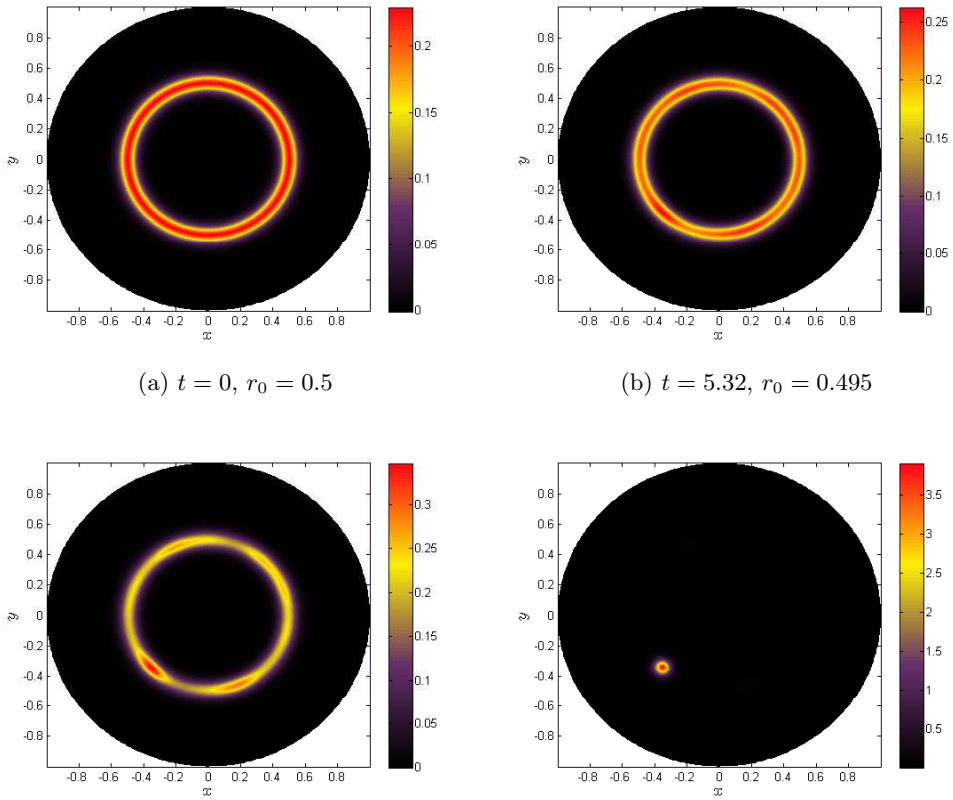

(a) $t = 0$, $r_0 = 0.5$

(b) $t = 5.32$, $r_0 = 0.495$

(c) $t = 6.32$, $r_0 = 0.493$

(d) $t = 10$, $r_0 = 0.493$

Figure 5.1: *Experiment 1:* Contour plot of the solution $v$ to (1.1) with ring geometry at four times with exponent set $(2, 1, 2, 0)$. The parameter values are $\epsilon = 0.025$, $D = 1$, $\tau = 0.1$, and $\sigma = 0$. The radius $r_0$ is computed as the average value of the radial positions corresponding to the maximum of $v$ for each $\theta$.

For our first experiment we take $D = 1$, $R = 1$, $r_0 = 0.5$, and $\epsilon = 0.025$. From Fig. 4.2, when $b = 0$, we predict $m_{\text{dom}} = 4.80$ and hence a four-spot breakup pattern. We plot the results from the simulation in Fig. 5.1, and from the Fourier transform in Fig. 5.2, where we see that $m = 4$ is one of the most dominant modes. The rather slow onset of the breakup can be attributed to the unstable eigenvalues in Fig. 4.2 being below $\lambda = 1$.

For the remainder of our numerical experiments we will study the effect of saturation ($\sigma \neq 0$), since by Proposition 4.3 it follows that without saturation breakup instabilities will occur for all parameter values. For experiment 2, we take the same parameter set as in experiment 1 but now take $\sigma = 25$. By (3.6), this corresponds to $b = 0.1356$ and, from Fig. 4.2, we do not anticipate this low value of the saturation to stabilize the breakup pattern. However, for this value of $b$ the instability band is significantly diminished and so we expect

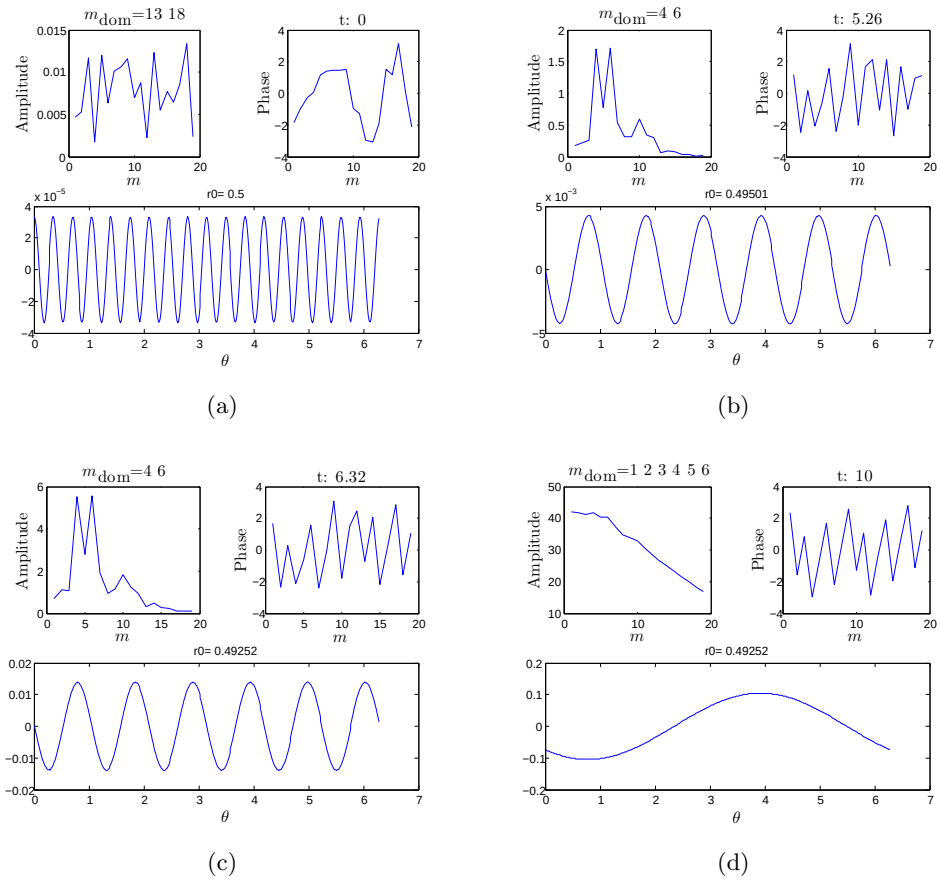


Figure 5.2: *Experiment 1:* Discrete Fourier transform of the solution $v$ to (1.1) with ring geometry at four times with exponent set $(2, 1, 2, 0)$. The parameter values are $\epsilon = 0.05$, $D = 1$, $\tau = 0.1$, and $\sigma = 0$. The upper left plot shows the amplitudes from the Fourier transform while the upper right plot displays the phase. The bottom graphic in each panel shows an inverse Fourier transform of a solution comprised of only the most dominant mode.

that the dominant mode for experiment 2, $m_{\rm dom} = 4.68$, should be more pronounced when compared to experiment 1, since there is less clustering near the dominant mode. Since the magnitude of the unstable eigenvalues with $\mathrm{Re}(\lambda) > 0$ decreases as well, this should lead to an increase in the time needed for breakup instability formation.

The results for experiment 2 are shown in Fig. 5.3, with the Fourier transform results given in Fig. 5.4. We notice that these predicted results do indeed hold, as the onset of instability is delayed when compared to Fig. 5.1 and the four spot breakup pattern is more pronounced. We also notice that the ring is thicker owing to the wider homoclinic orbit solution that occurs as $b$ increases (cf. [17]). Finally, we note that since the initial radius, $r_0 = 0.5$ is greater than the equilibrium value predicted by (3.7) for the parameter set used in experiment 2, the ring

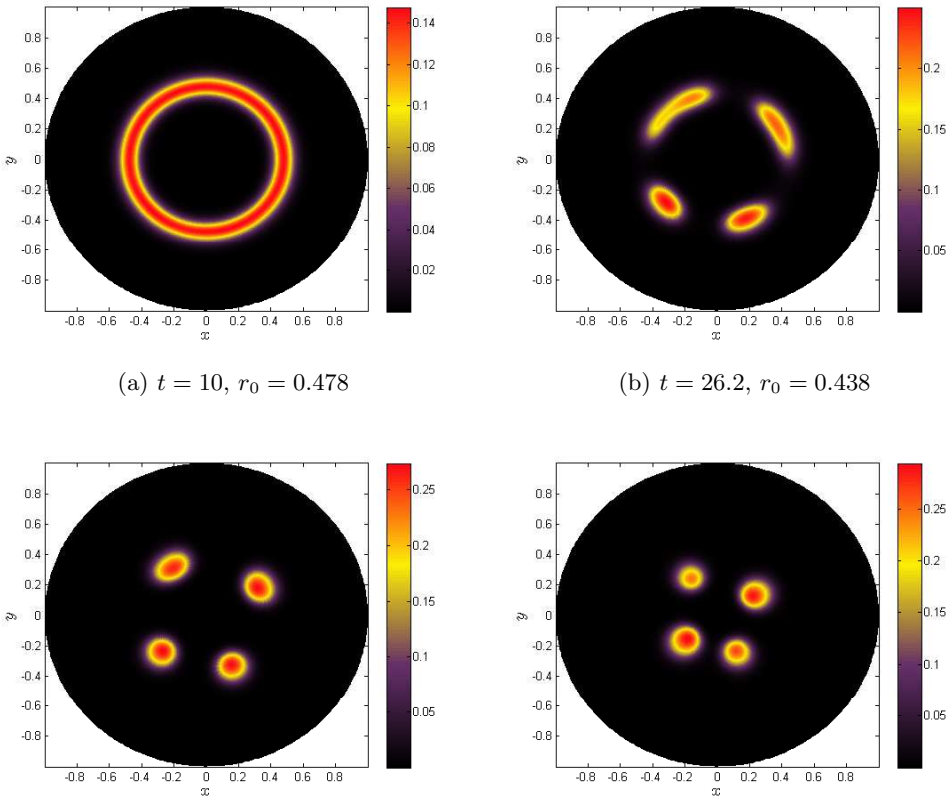

(a) $t = 10$, $r_0 = 0.478$

(b) $t = 26.2$, $r_0 = 0.438$

(c) $t = 37.3$, $r_0 = 0.358$

(d) $t = 50$, $r_0 = 0.243$

Figure 5.3: *Experiment 2:* Contour plot of the solution $v$ to (1.1) with ring geometry at four times with exponent set $(2, 1, 2, 0)$. The parameter values are $\epsilon = 0.025$, $D = 1$, $\tau = 0.1$, and $\sigma = 25$. The radius $r_0$ is computed as the average value of the radial positions corresponding to the maximum of $v$ for each $\theta$.

radius should decrease. Indeed we see over the course of the experiment that $r_0$ decreases to $r_0 \approx 0.48$ before breakup up occurs.

For experiment 3, we once again take the same parameters as in experiment 1 but with $\sigma = 950$. Then, from (3.6), we get $b = 0.2010$ and, by Fig. 4.2, we predict that there is no longer any breakup instability. Therefore, after an initial transient period where the ring thickens due to the saturation, the ring should remain relatively static with dynamics only occurring due to (3.7). Once again, the initial radius $r_0 = 0.5$ is greater than the equilibrium value and so the radius should decrease. By Fig. 3.1, $b$ increases as $r_0$ decreases and this should cause the ring to thicken even further. Indeed, all of this predicted behaviour is evidenced in Fig. 5.5. The Fourier transform plot shown in Fig. 5.6 indicates that, while $m = 4$ remains the dominant integer mode, the Fourier amplitudes do decrease over time, and so no breakup

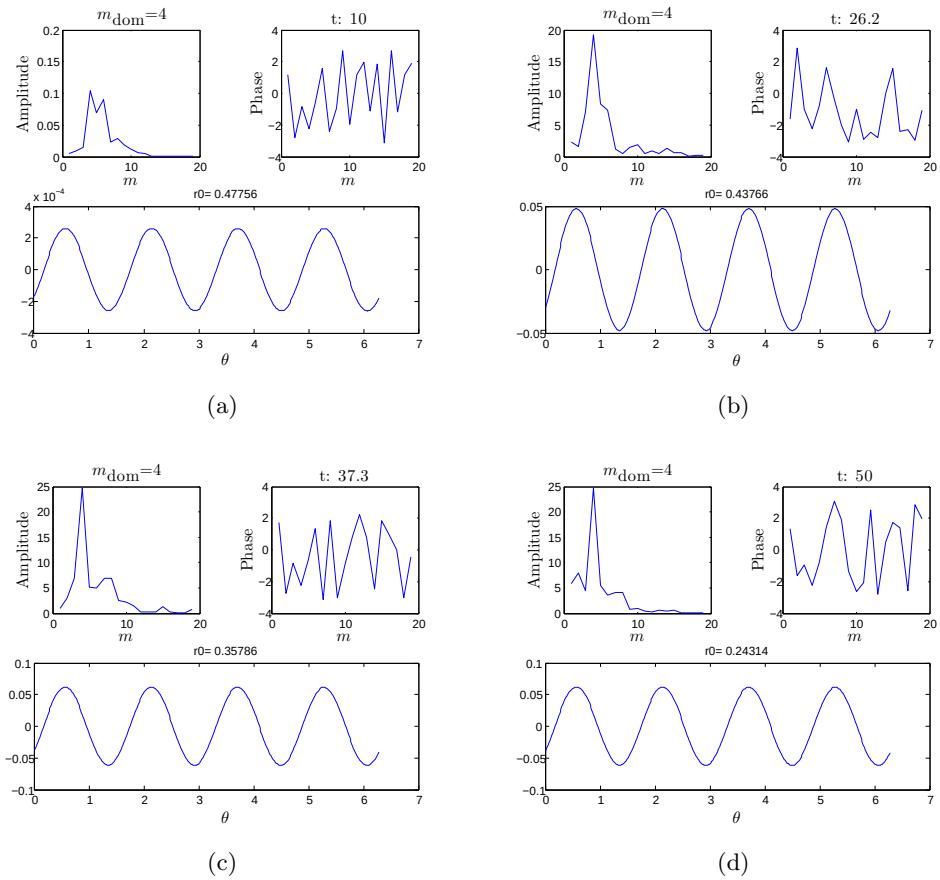


Figure 5.4: *Experiment 2:* Discrete Fourier transform of the solution $v$ to (1.1) with ring geometry at four times with exponent set $(2, 1, 2, 0)$. The parameter values are $\epsilon = 0.025$, $D = 1$, $\tau = 0.1$, and $\sigma = 25$.

instability occurs.

Finally, we consider two experiments where we illustrate our results regarding zig-zag instabilities. For experiment 4 we take the parameters as in experiment 3 but now use, as an initial perturbation, localization on a curve of radius $r = 0.5 + 0.02\cos(6\theta)$. We predicted in Principal Result 3.2 that when $r_0 \ll 1$, the velocity corrections are in phase with the perturbations and should lead to curve stabilization. The full numerical results shown in Fig. 5.7 do illustrate this circularization tendency of the curve. However, when $r_0 \gg 1$, we can no longer guarantee that curve perturbations will circularize. To illustrate this, in experiment 5 we take the parameter set $D = 0.01$, $r_0 = 0.5$, and $\epsilon = 0.01$. At first glance it looks like the same behaviour could occur because the same computational value of $r_0$ has been chosen as in experiment 4. However, the diffusivity has changed and if we scale to $D = 1$, the equivalent problem would be $R = 10$, $r_0 = 5$, and $\epsilon = 0.1$. Since varying the parameters does affect the

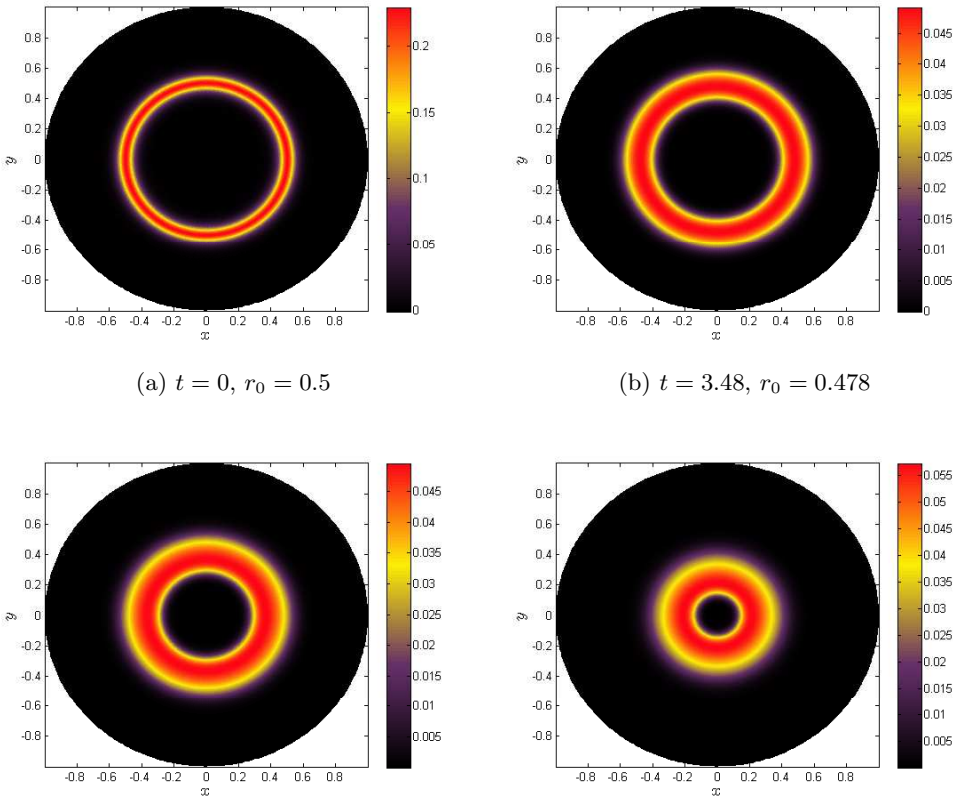

(a) $t = 0$, $r_0 = 0.5$

(b) $t = 3.48$, $r_0 = 0.478$

(c) $t = 12.2$, $r_0 = 0.365$

(d) $t = 20$, $r_0 = 0.213$

Figure 5.5: *Experiment 3:* Contour plot of the solution $v$ to (1.1) with ring geometry at four times with exponent set $(2, 1, 2, 0)$. The parameter values are $\epsilon = 0.025$, $D = 1$, $\tau = 0.1$, and $\sigma = 950$. The radius $r_0$ is computed as the average value of the radial positions corresponding to the maximum of $v$ for each $\theta$.

saturation value $\sigma$, we need to take $\sigma = 5910$ in order to use $b = 0.210$, which is the value used in experiment 3 and experiment 4. Fig. 5.8 show the results of this experiment where the curve begins to accentuate the small angular perturbations causing overall curve lengthening that destabilizes the circular solution. However, this new solution does not undergo any breakup instabilities as it evolves. It is worth mentioning that the parameters chosen for experiment 5 are very similar to those chosen in Fig. 2.1c where the algorithm developed in [26] was used to demonstrate curve buckling. Therefore, perhaps tuning the saturation parameter if necessary, it is reasonable to expect that such a pattern would be stable to breakup based on experiment 5.

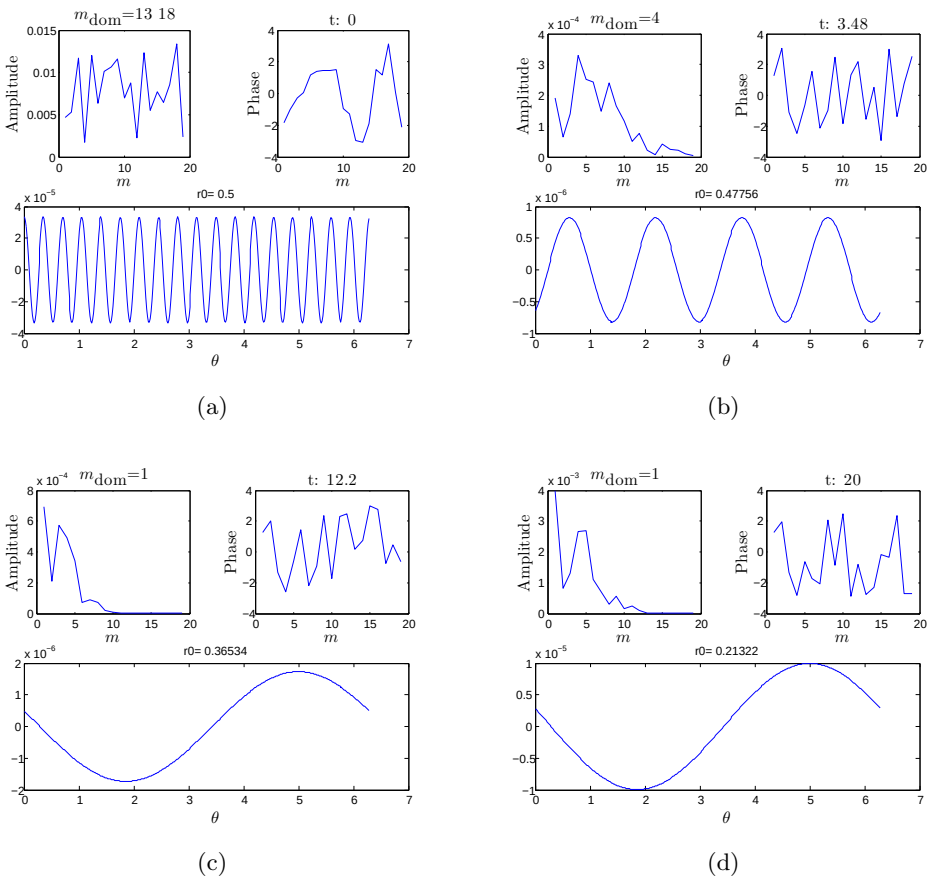


Figure 5.6: *Experiment 3:* Discrete Fourier transform of the solution $v$ to (1.1) with ring geometry at four times with exponent set $(2, 1, 2, 0)$. The parameter values are $\epsilon = 0.05$, $D = 1$, $\tau = 0.1$, and $\sigma = 950$.

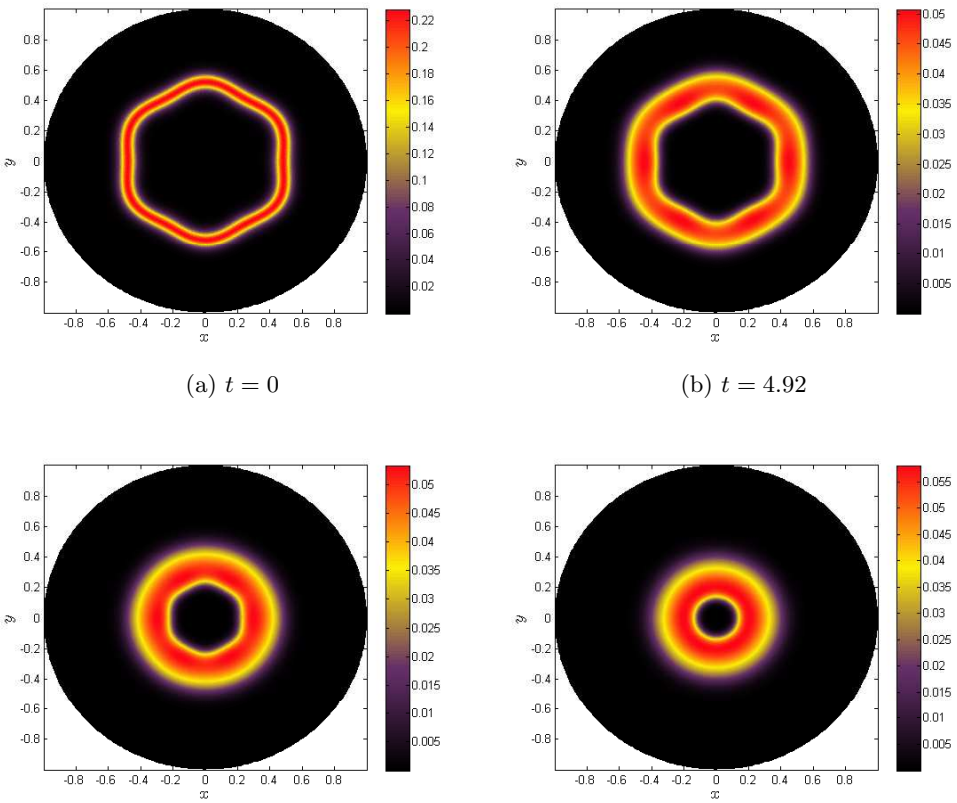

(a) $t = 0$ (b) $t = 4.92$

(c) $t = 15.76$ (d) $t = 20$

Figure 5.7: *Experiment 4:* Contour plot of the solution $v$ to (1.1) with perturbed ring geometry of the form $\cos(6\theta)$ at four times with exponent set $(2, 1, 2, 0)$. The parameter values are $\epsilon = 0.025$, $D = 1$, $\tau = 0.1$, and $\sigma = 950$. The radius $r_0$ is computed as the average value of the radial positions corresponding to the maximum of $v$ for each $\theta$.

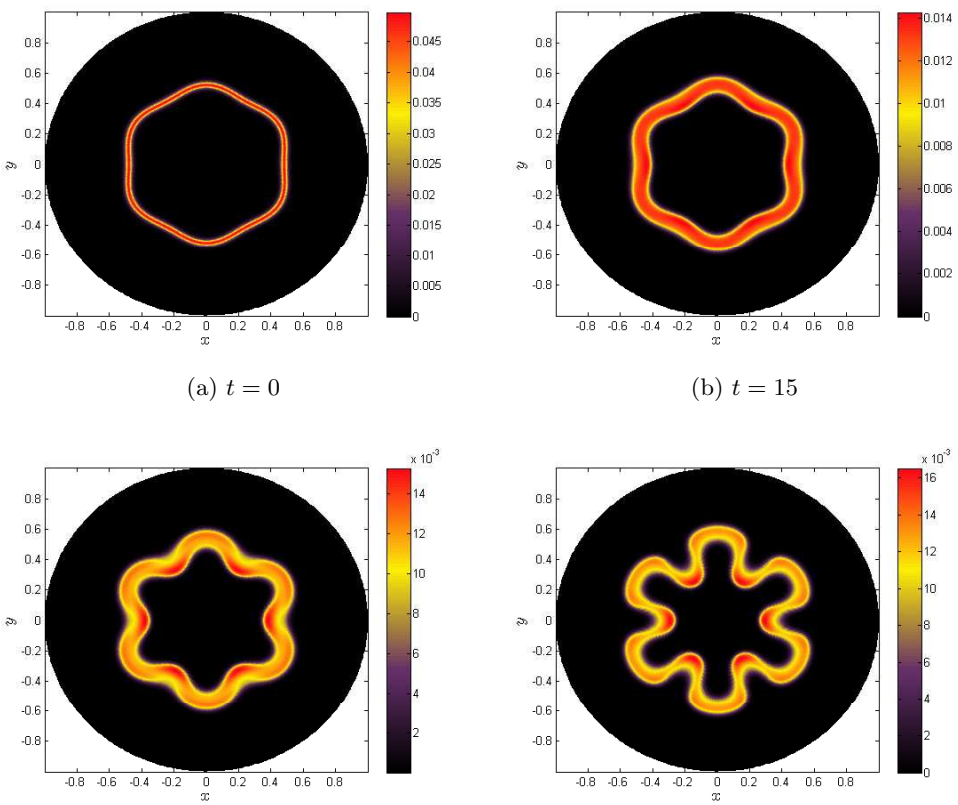

(a) $t = 0$ (b) $t = 15$

(c) $t = 31$ (d) $t = 50$

Figure 5.8: *Experiment 5:* Contour plot of the solution $v$ to (1.1) with perturbed ring geometry of the form $\cos(6\theta)$ at four times with exponent set $(2, 1, 2, 0)$. The parameter values are $\epsilon = 0.01$, $D = 0.01$, $\tau = 0.1$, and $\sigma = 5910$. This corresponds to a scaling of the problem $D = 1$, $\epsilon = 0.1$, $R = 10$, and $\tau = 0.1$. We take as an initial base radius $r_0 = 0.5$ which scales to $r = 5$ when $D = 1$. The radius $r_0$ is computed as the average value of the radial positions corresponding to the maximum of $v$ for each $\theta$.

**6. Discussion.** We have analyzed a singularly perturbed RD system in the semi-strong diffusion regime in two spatial dimensions where an activator species is localized to a closed curve, while the inhibitor species exhibits global behaviour over the domain. In this semi-strong asymptotic limit, we derived a novel moving boundary problem characterizing the slow time evolution of the curve, which is defined in terms of a quasi steady-state inhibitor diffusion field and its properties on the curve. Since this curve-evolution problem differs significantly from the traditional mean curvature flows and quasi-static moving boundary problems common in the field of materials science, in the companion article [26] a new numerical methodology was developed to compute curve evolution from this new quasi-static moving BVP.

The qualitatively interesting numerical results from this curve evolution problem, as shown in Fig. 2.1, provided motivation for our detailed analysis of the existence, stability, and dynamics, of ring and near-ring solutions to the GMS model in radially symmetric geometries. A brief summary of some of our major findings for this class of ring solutions is as follows: We first showed that, in contrast to the saddle-node bifurcation structure for steady-state ring solutions in the absence of activator saturation, the introduction of the saturation parameter admits a hysteresis effect between two stable branches of ring-equilibria, and that ring-equilibria now exist for all ring radii. Secondly, we used our curve evolution problem to show that, for the case of near-ring solutions, a perturbed ring will ultimately circularize if the ring radius is small enough. In addition, a higher order theory was developed to determine the mean drift of a perturbed ring. Thirdly, in our stability analysis of a ring solution, we showed that the breakup instability band, which triggers the disintegration of a ring into localized spots, can disappear when the saturation parameter is sufficiently large. Therefore, under sufficiently large activator saturation, the slow curve evolution problem should accurately reflect corresponding behavior in the full PDE system. Finally, we provided a new matched asymptotic expansion analysis to derive an explicit formula for the small eigenvalues of order $\mathcal{O}(\epsilon^2)$ of the linearization of the ring solution, which characterize any zig-zag shape-deforming instabilities of the curve. The calculation of such eigenvalues is a new result, and due to the non-zero curvature of the ring the analysis was considerably more intricate than that for a straight stripe solution performed previously in [17]. Moreover, these eigenvalues were shown to agree with the normal velocity corrections to the perturbed near-ring dynamics. Our full numerical results in §5 computed from the RD system for the GMS model demonstrated predicted breakup modes in the absence of saturation, as well as the stabilizing effect that saturation has on such patterns. These results also showed the predicted curve circularization tendency for perturbed circles of small radii, and the initial development of labyrinthian-shaped curve for perturbed rings of a large enough radius, or if the inhibitor diffusion coefficient is appropriately scaled.

Finally, we briefly discuss four open directions that warrant further investigation. One particular challenging problem is to derive and then analyze a nonlocal eigenvalue problem (NLEP) whose spectrum will characterize the possibility of $\mathcal{O}(1)$ time-scale breakup instabilities for an arbitrary closed curve in the semi-strong interaction limit. The formulation of this linear stability problem would, at least for low wavelength perturbations, involve the full numerical solution of a free boundary problem for the linearization of the inhibitor field. We anticipate that a hybrid asymptotic-numerical approach would be required to analyze the

spectrum of the NLEP. One of the challenges to this is that the boundary coordinate Laplace operator is not separable and as such the eigenfunction expansion is cumbersome. However, we showed for a ring that high curvature tends to stabilize the breakup instability pattern and conjectured that this would hold for arbitrary curves. Taking a high curvature limit of the boundary coordinate operator may simplify the resulting linear stability problem and allow for an analytic insight to the upper stability band in a similar fashion to the ring problem.

A second open direction would be extending our analysis of near ring solutions to a related problem of a circular curve in a domain with a boundary that is only slightly perturbed from a circle. This would easily fit into the numerical curve tracking algorithm presented in [26] and would provide an interesting case for comparison to the results presented here, particularly in regards to geometry effects on stability threshold. A third interesting open problem would be moving beyond the study of closed curve-evolution to the case where the curve is not closed, but instead has endpoints, or tips, inside the domain. The analysis of localized pattern formation in the presence of these stripe fragments is largely an open problem (see [1] for one specific study). It would be interesting to develop an asymptotic approach to derive a reduced dynamical description of tip dynamics through the asymptotic matching of the local tip behavior to the global inhibitor field. Finally, it would be worthwhile to develop a hybrid asymptotic-numerical approach to study localized pattern formation for the GMS model in the weak interaction regime, where $D = \mathcal{O}(\epsilon^2)$. The numerical experiment shown in Fig. 5.8 gives a glimpse that rather intricate dynamics should occur in this regime. With this scaling, both problems are localized and so it will be easier to formulate analytical problems for both the equilibrium and stability of arbitrary curves. However, like with the NLEP formulation in the semi-strong region presented here, numerical techniques will be required for determining stability boundaries.

## REFERENCES

[1] D Andreucci, M. A. Herrero, and J. J. L. Velazquez, *On the growth of filamentary structures in planar media*, Math Methods in the Appl. Sci., 27 (2004), pp. 1935–1968.
[2] P. W. Bates and J. Shi, *Existence and instability of spike layer solutions to singular perturbation problems*, J. Funct. Anal., 196 (2002), pp. 211–264.
[3] C. M. Bender and S. A. Orszag, *Advanced Mathematical Methods for Scientists and Engineers I: Asymptotic Methods and Perturbation Theory*, vol. 1, Springer, 1999.
[4] H. Berestycki and P. L. Lions, *Nonlinear scalar field equations. I. Existence of a ground state*, Arch. Rat. Mech. Anal., 82 (1983), pp. 313–345.
[5] V. F. Breña-Medina, D. Avitabile, A. R. Champneys, and M. J. Ward, *Stripe to spot transition in a plant root hair initiation model*, SIAM J. Appl. Math., 75 (2015), pp. 1090–1119.
[6] W. Chen and M. J. Ward, *Oscillatory instabilities and dynamics of multi-spike patterns for the one-dimensional Gray-Scott model*, Europ. J. Appl. Math., 20 (2009), pp. 187–214.
[7] ———, *The stability and dynamics of localized spot patterns in the two-dimensional Gray-Scott model*, SIAM J. Appl. Dyn. Sys., 10 (2011), pp. 582–666.
[8] A. Doelman, R. A Gardner, and T. J. Kaper, *Large stable pulse solutions in reaction diffusion equations*, in Indiana U. Math. J, 2000.
[9] A. Doelman, T. J. Kaper, and K. Promislow, *Nonlinear asymptotic stability of the semistrong pulse dynamics in a regularized Gierer-Meinhardt model*, SIAM J. Math. Anal., 38 (2007), pp. 1760–1787.
[10] A. Doelman and H. van der Ploeg, *Homoclinic stripe patterns*, SIAM J. Appl. Dyn. Sys., 1 (2002), pp. 65–104.

[11] P. C. Fife, *Dynamics of Internal Layers and Diffusive Interfaces*, vol. 53, SIAM, 1988.
[12] A. Gierer and H. Meinhardt, *A theory of biological pattern formation*, Kybernetik, 12 (1972), pp. 30–39.
[13] K. B Glasner and A. E Lindsay, *The stability and evolution of curved domains arising from one-dimensional localized patterns*, SIAM J. Appl. Dyn. Sys., 12 (2013), pp. 650–673.
[14] D. Iron and M. J. Ward, *The dynamics of multispike solutions to the one-dimensional Gierer–Meinhardt model*, SIAM J. Appl. Math., 62 (2002), pp. 1924–1951.
[15] D. Iron, M. J. Ward, and J. Wei, *The stability of spike solutions to the one-dimensional Gierer–Meinhardt model*, Physica D, 150 (2001), pp. 25–62.
[16] A. J. Koch and H. Meinhardt, *Biological pattern formation: From basic mechanisms to complex structures*, Reviews of Modern Physics, 66 (1994), p. 1481.
[17] T. Kolokolnikov, W. Sun, M. J. Ward, and J. Wei, *The stability of a stripe for the Gierer-Meinhardt model and the effect of saturation*, SIAM J. Appl. Dyn. Sys., 5 (2006), pp. 313–363.
[18] T. Kolokolnikov, M. J. Ward, and J. Wei, *The existence and stability of spike equilibria in the one-dimensional GrayScott model: The low feed-rate regime*, Studies in Appl. Math., 115 (2005), pp. 21–71.
[19] ———, *Spot self-replication and dynamics for the Schnakenburg model in a two-dimensional domain*, J. Nonlin. Sci., 19 (2009), pp. 1–56.
[20] T. Kolokolnikov and J. Wei, *On ring-like solutions for the Gray–Scott model: Existence, instability and self-replicating rings*, Europ. J. Appl. Math., 16 (2005), pp. 201–237.
[21] T. Kolokolnikov, J. Wei, and M. Winter, *Existence and stability analysis of spiky solutions for the Gierer–Meinhardt system with large reaction rates*, Physica D, 238 (2009), pp. 1695–1710.
[22] T. Kolokolnikov, J. Wei, and W. Yang, *On large ring solutions for Gierer–Meinhardt system in R3*, J. Diff. Eq., 255 (2013), pp. 1408–1436.
[23] C. S. Lin, W. M. Ni, and I. Takagi, *Large amplitude stationary solutions to a chemotaxis system*, J. Diff. Eq., 72 (1988), pp. 1–27.
[24] H. Meinhardt, *Models of Biological Pattern Formation*, vol. 6, Academic Press London, 1982.
[25] I. Moyles, W. H. Tse, and M. J. Ward, *Explicitly solvable nonlocal eigenvalue problems and the stability of localized stripes in reaction-diffusion systems*, Studies in Appl. Math., 136 (2016), pp. 89–136.
[26] I. Moyles and B. Wetton, *A numerical framework for singular limits of a class of reaction diffusion problems*, J. Comput. Phys., 300 (2015), pp. 308–326.
[27] C. B. Muratov and V. V. Osipov, *Stability of the static spike autosolitons in the Gray–Scott model*, SIAM J. Appl. Math., 62 (2002), pp. 1463–1487.
[28] Y. Nec and M. J. Ward, *An explicitly solvable nonlocal eigenvalue problem and the stability of a spike for a sub-diffusive reaction-diffusion system*, Math. Model. Nat. Phen., 8 (2013), pp. 55–87.
[29] W. M. Ni and J. Wei, *On positive solutions concentrating on spheres for the Gierer–Meinhardt system*, J. Diff. Eq., 221 (2006), pp. 158–189.
[30] Y. Nishiura and D. Ueyama, *A skeleton structure of self-replicating dynamics*, Physica D, 130 (1999), pp. 73–104.
[31] ———, *Spatio-temporal chaos for the Gray–Scott model*, Physica D, 150 (2001), pp. 137–162.
[32] K. J. Painter, P. K. Maini, and H. G. Othmer, *Stripe formation in juvenile pomacanthus explained by a generalized turing mechanism with chemotaxis*, PNAS, 96 (1999), pp. 5549–5554.
[33] J. E. Pearson, *Complex patterns in a simple system*, Science, 261 (1993), pp. 189–192.
[34] P. Prusinkiewicz, D. R. Fowler, and H. Meinhardt, *The Algorithmic Beauty of Sea Shells*, Springer Science & Business Media, 2009.
[35] X. Ren and J. Wei, *Oval shaped droplet solutions in the saturation process of some pattern formation problems*, SIAM J. Appl. Math., 70 (2009), pp. 1120–1138.
[36] E. B. Saff and A. D. Snider, *Fundamentals of Complex Analysis for Mathematics, Science, and Engineering*, Prentice-Hall, 1976.
[37] M. B. Short, G. O. Mohler, P. J. Brantingham, and G. E. Tita, *Cops on the dots in a mathematical model of urban crime and police response*, DCDS-B, 19 (2014).
[38] A. Turing, *The chemical basis of morphogenesis*, Phil. Trans. Royal Soc. London. Series B, Biological Sciences, 237 (1952), pp. 37–72.

[39] J. C. Tzou, M. J. Ward, and T. Kolokolnikov, *Slowly varying control parameters, delayed bifurcations, and the stability of spikes in reaction-diffusion systems*, Physica D, 190 (2015), pp. 24–43.
[40] M. J. Ward and J. Wei, *Hopf bifurcations and oscillatory instabilities of spike solutions for the one-dimensional Gierer-Meinhardt model*, J. Nonlin. Sci., 13 (2003), pp. 209–264.
[41] J. Wei, *On single interior spike solutions of the Gierer–Meinhardt system: Uniqueness and spectrum estimates*, Europ. J. Appl. Math., 10 (1999), pp. 353–378.
[42] J. Wei and M. Winter, *A nonlocal eigenvalue problem and the stability of spikes for reaction–diffusion systems with fractional reaction rates*, Inter. J. Bifur. Chaos, 13 (2003), pp. 1529–1543.
[43] ———, *On the Gierer–Meinhardt system with saturation*, Commun. Cont. Math., 6 (2004), pp. 259–277.